UCRL-11563
c.2

University of California

Ernest O. Lawrence Radiation Laboratory

TWO-WEEK LOAN COPY

This is a Library Circulating Copy
which may be borrowed for two weeks.
For a personal retention copy, call
Tech. Info. Division, Ext. 5545

RECOIL STUDIES OF NUCLEAR REACTIONS OF Ir, Bi AND Pb^{208} WITH O^{16}

Berkeley, California

UCRL-11563
c.2

DISCLAIMER

This document was prepared as an account of work sponsored by the United States Government. While this document is believed to contain correct information, neither the United States Government nor any agency thereof, nor the Regents of the University of California, nor any of their employees, makes any warranty, express or implied, or assumes any legal responsibility for the accuracy, completeness, or usefulness of any information, apparatus, product, or process disclosed, or represents that its use would not infringe privately owned rights. Reference herein to any specific commercial product, process, or service by its trade name, trademark, manufacturer, or otherwise, does not necessarily constitute or imply its endorsement, recommendation, or favoring by the United States Government or any agency thereof, or the Regents of the University of California. The views and opinions of authors expressed herein do not necessarily state or reflect those of the United States Government or any agency thereof or the Regents of the University of California.

UCRL-11563

UNIVERSITY OF CALIFORNIA

Lawrence Radiation Laboratory
Berkeley, California

AEC Contract No. W-7405-eng-48

RECOIL STUDIES OF NUCLEAR REACTIONS OF Ir, Bi AND Pb^{208} WITH O^{16}

Paul D. Croft

(Ph.D. Thesis)

July 20, 1964

Printed in USA. Price $2.00. Available from the
Office of Technical Services
U. S. Department of Commerce
Washington 25, D.C.

RECOIL STUDIES OF NUCLEAR REACTIONS OF Ir, Bi AND Pb^{208} WITH O^{16}

Contents

Abstract v

I. Introduction 1

II. Experimental Procedures, Analyses and Results 5

A. Bombardments of Natural Iridium; Aluminum Catcher Foils 9

B. Bombardments of Natural Iridium; Aluminum Oxide Catcher Foils 11

C. Bombardments of Bi^{209} and Pb^{208}; Aluminum Oxide Catcher Foils 12

D. Bombardments of Bi^{209} and Pb^{208}; Angular Distribution Experiments 15

III. Discussion 20

A. Range-Energy Curves for At, Po Recoils 20

B. Nuclear Reactions 26

IV. Conclusions 38

Acknowledgments 39

Tables 40

Figures 52

Appendices 71

A. Analysis of Pulse-Height Spectra of Al_2O_3 Foils from Bi and Pb Bombardments 71

B. Radon Diffusion 78

C. Errors 80

Footnotes and References 85

RECOIL STUDIES OF NUCLEAR REACTIONS OF Ir, Bi, and Pb^{208} WITH O^{16}

Paul D. Croft

Lawrence Radiation Laboratory
University of California
Berkeley, California

July 20, 1964

ABSTRACT

Range energy curves for 6 to 12 MeV At and Po recoils in Al leaf and Al_2O_3 have been determined using nuclear reactions of O^{16} with Ir to produce the recoils. Al leaf foils of ~0.15 mg/cm^2 and Al_2O_3 foils of 0.07 mg/cm^2 were used. Ranges in mg/cm^2 are 7 to 11% larger in Al_2O_3 than in Al. The range energy curves obtained were compared with theoretical predictions and were used to transform measured ranges for Po, At, Rn and Fr into recoil energies.

Projected range distributions in stacked Al_2O_3 foils were determined for the α-active products from the reactions $Bi^{209}(O^{16},X)Y$ at various bombarding energies from 76 to 163 MeV and $Pb^{208}(O^{16},X)Y$ at 123 and 163 MeV. The products, Y, identified were $Po^{206,208,210}$, $At^{209,211}$, $Rn^{210,211,212}$ and Fr^{212}.

The nature of X could be exactly specified only for the Bi bombardments near the Coulomb barrier where the results indicate that Po^{210} and At^{211} are formed by p and 2p transfers, with the residual N^{15} and C^{14} being ejected in a preferentially backward direction. These processes give the recoils energies and ranges up to about 3 times the values possible from a compound nucleus reaction. For both Pb and Bi targets at bombarding energies above about 1.3 times the Coulomb barrier, the range distributions for the products generally peak at ranges from one-quarter to one-half the compound nucleus range, but most have a long-range tail. With the help of angular distribution experiments, it was possible to clarify in a qualitative way the mechanisms at the higher energies. No evidence was obtained which indicates that α transfer might be a preferred mode.

I. INTRODUCTION

Reactions which involve transfer of one or more nucleons between an incident heavy ion and a target nucleus can be divided into two groups. In the first group, we can place complete amalgamation of the two nuclei to form what is usually called the compound nucleus. This term, "compound nucleus", has met with some undiscriminating use in the past. Zucker has discussed the problem and describes a compound nucleus reaction as one "in which [the projectile and target]...have merged and small fragments are emitted as a means of de-excitation."[1] With the stipulation that fission is also an acceptable means of de-excitation, this definition is the one used for purposes of this paper. Clearly, compound nucleus formation implies total momentum transfer (TMT); that is, the compound nucleus assumes the total momentum of the projectile.

The second group consists of partial momentum transfer (PMT) reactions. At high impact parameters, single-nucleon transfer, often preceded by Coulomb excitation, can occur. These single-nucleon transfer reactions have been widely investigated, and they have been treated with reasonable success by the tunneling theory of Breit and Ebel, at least for incident energies which do not greatly exceed the Coulomb barrier.[1-4] At lower impact parameters, presumably, multi-nucleon transfers occur; the grazing model was proposed by Kaufman and Wolfgang to help describe these results.[5] Single- and multi-nucleon transfers have been observed in both directions—projectile-to-target and target-to-projectile. Some PMT reactions, for example $Mg^{26}(N^{14},N^{13})Mg^{27}$ as studied by Halbert et al., result in coherent products.[6] In others, breakup into showers of smaller particles apparently occurs.[7,8]

Studies of PMT reactions can be made in two general ways. Consider the case of transfer from incident particle to target nucleus. One can examine the residue(s) of the projectile not abosrbed into the target, or one can examine the product(s) resulting from the de-excitation

of the conglomerate (target + transferred matter). These examinations can also take two forms. The products can be counted directly with solid state detectors or can be identified, if radioactive, by their decay modes. These four techniques should not be compared with the idea of finding a "best" method. Each can provide specific information about some phase of the nuclear reaction. Indeed, the four methods are highly complementary.

The approach of the work reported here was to measure recoil ranges and straggling, cross sections and angular distributions of certain radioactive products from the conglomerate heavy nucleus formed after transfer. The projectile was O^{16}; Bi^{209} and Pb^{208} were selected as targets for a number of reasons. First, in the mass region where one would expect to find the products of PMT reactions, there are several α-active nuclides with convenient half lives.[9] Alpha-particle counting has advantages not common to measurements of other types of radiation. Since counter backgrounds can be reduced to very low levels, the method is sensitive to products of low yield. Furthermore, if thin enough catcher foils are used the α particles emitted from the stopped products are not substantially degraded; detection and pulse-height analysis then can yield measurements of a number of different nuclides without the necessity of chemical separations or resolution of decay curves. In this work, $Po^{206,208,210}$, $At^{209,211}$, $Rn^{210,211,212}$, and Fr^{212} were readily identified when present; upper limits could be set for the yields of $Rn^{208,209}$ and At^{207}; low α-branching ratios precluded measurements of Po^{207} and At^{210} and a very long half life made Po^{209} undetectable.

Another motivation for the choice of Bi and Pb as targets came from various heavy element fission results. Viola and Sikkeland found that the total fission cross sections for 166 MeV O^{16} + U^{238} agreed well both with the total reaction cross section calculated by Thomas and with extrapolation of the experimentally measured total reaction cross sections of Wilkins and Igo.[10-12] Momentum transfer measurements

by Viola and Sikkeland showed that while most of the fission events came from TMT reactions, up to 30% resulted from PMT reactions corresponding to transfer of an α particle or, at least, "four nucleons".[13,14] For the 166 MeV O^{16} + Bi^{209} reaction, on the other hand, the same workers found no evidence for PMT reactions leading to fission.[13] Moreover, the total fission cross section for O^{16} + Bi was measured by Britt and Quinton to be only about 72% of the total reaction cross section.[15] This suggests that PMT reactions on Bi do occur but, unlike the U^{238} case, do not lead to fission. Thus, they might be expected to contribute to the α-active products described above.

Alexander and Winsberg, using a stacked foil technique, indeed found that most of the α-active products from high energy O^{16} + Bi bombardments had recoil ranges substantially less than that expected for the TMT compound nucleus products.[16] They also suggested α transfer to account for these results. They measured only gross activity, however, and were able to identify only one product—At^{211} produced at low projectile energies.

For the present work, stacked foil techniques were used, supplemented with the α-energy analysis mentioned earlier so that the production of individual nuclides was studied. These range studies, along with angular distribution measurements, yield useful information about the momentum transferred in a reaction, and thence help elucidate the mechanism. Al leaf catcher foils, used successfully by many workers,[17-21] were found to be too thick to allow adequate resolution of the many α groups present. Thinner foils made of Al_2O_3 were then substituted.[22] Range-energy curves for At, Po recoils in Al and Al_2O_3 were determined experimentally; the recoils were produced by bombarding Ir targets with O^{16} ions. A variety of considerations lead one to expect that the At and Po from such a reaction result from TMT compound nucleus formation; thus the energy of the recoils is known. The first O^{16} + Bi experiments performed verified that very few α-active products had ranges as long as the TMT range. This implies that the compound

nucleus, as expected, is not contributing to the α-active products but is largely decaying by some other process—namely fission. Alpha-particle transfer was suggested by the fact that many of the observed range distributions peaked at about one-quarter the TMT range; however, in the O^{16} + Bi experiments the presence of Rn isotopes (three protons above the target) immediately indicated that α transfer, if present, was not unique. In fact, the presence of multiple peaking in some range distributions suggested that some of the observed nuclides were being produced by more than one mechanism. Moreover, the most probable range for some products changed with energy in such a way as to indicate that different mechanisms were operative at different energies. In order to get a survey of the apparently complex PMT reactions, range distributions for as many products as possible were obtained for the reactions of O^{16} with Bi^{209} at a number of bombarding energies between 76 and 163 MeV. Similar distributions were obtained for the reactions of O^{16} with Pb^{208} at 123 and 163 MeV. In addition, rough angular distribution measurements were made for both Bi and Pb targets at both 123 and 163 MeV.

In summary then, this work represents an exploratory study using recoil range techniques, of those reactions of O^{16} with Ir, Bi, and Pb^{208} which produce α emitters of half lives between 5 min and 3 yrs. Because of the complexity of competing and interfering reactions, in only a few cases was it possible to positively assign the production of a given nuclide to a specific reaction. However, the results do shed some light on the general features of reactions of heavy ions with heavy elements, and can be used to guide further investigations.

II. EXPERIMENTAL PROCEDURES, ANALYSES AND RESULTS

The experiments can be classified into four general types, all with O^{16} as projectile: (a) Ir targets with stacked Al catcher foils; (b) Ir targets with stacked Al_2O_3 catcher foils; (c) Bi and Pb^{208} targets with stacked Al_2O_3 catcher foils; (d) angular distribution measurements with Bi and Pb^{208} targets. Certain features of the four types of experiment were similar or identical; these will be described first. The differentiating characteristics are discussed in subsequent sections.

The errors associated with the various quantities measured are given along with the quantity only when convenient or necessary to the immediate discussion. Error estimates are collected and discussed in Appendix C.

Bombarding Particle Source. The oxygen beams used were provided by the Berkeley Heavy Ion Linear Accelerator (Hilac) which produces heavy ion beams of 10.4 ± 0.2 MeV/amu.[23] Aluminum degraders were introduced before the target when beams of lower energy were desired. The range-energy curves of Northcliffe were used to determine the energy of the degraded beam.[24] Bending magnets were used to extract the beam from the main axis of the machine and these also defined the charge state of the beam particles. The beam was collimated through two 3/16 in. diameter holes placed ten inches apart, the second being just before the target. Beam monitoring was achieved with a Faraday cup and electrometer. When higher accuracy was required, a cylindrical magnet was placed around the cup to minimize interference from scattered electrons.

Targets. Targets were prepared by vacuum evaporation of the desired metal through a collimating hole onto 0.00025 in. aluminum foil. Target thicknesses were about 40 to 140 $\mu g/cm^2$ and were obtained from area and weight determinations. Most of the targets were made by Daniel J. O'Connell of this Laboratory.

Catcher Foils. Two materials were used for catcher foils. The aluminum foils were punched from aluminum leaf with a circular punch of accurately known area (5.07_5 cm^2) and weighed. Thicknesses were about 120 to 160 $\mu g/cm^2$. This method of measurement of the thickness assumes that the foils were uniform over the entire area. The thicknesses obtained indicated an average gradient of less than 9 $\mu g/cm^2$ per cm; this result agrees well with that of Alexander and Winsberg for similar aluminum leaf.[17] Each foil was examined before a bright light so that those with an inordinately large number of pin holes could be rejected.

The aluminum oxide catchers were made by the method of Harris.[25] Strips about 1 in. by 2 in. of ordinary household aluminum foil were anodized on both sides to the required thickness of Al_2O_3 in an aqueous ammonium citrate solution. After washing and drying stages, the foils were sandwiched between thin stainless steel rings (1.125 in. o.d., 0.875 in i.d. Early in the work, the rings were 0.018 in. thick; later 0.010 in. rings were used). The three pieces were firmly spotwelded together and the excess foil trimmed away (see Fig. 1). A circle of 10 N NaOH approximately 3/4 in. in diameter was painted on one of the anodized surfaces. This removes the oxide layer from that side and begins to etch the Al layer beneath. After a few minutes excess NaOH was washed off and the sandwich was dipped in 8 N HCl until the exposed Al was dissolved. The resulting package required rather careful handling until thorough washing (H_2O; H_2O and alcohol; acetone) and drying steps were completed. Subsequently, normally careful treatment allowed survival of almost all foils.

Although the Al_2O_3 foils were slightly more difficult to produce than foils of Al leaf, they were found to be generally more satisfactory for this work. There were two main advantages: (i) The Al_2O_3 foils could be made thinner than those of aluminum. Thus, substantially better resolution of the alpha spectra could be obtained. (ii) Once the long-lived activity (if any) in an Al_2O_3 catcher was determined, the foil

could be re-used. The handling and mounting procedures required for counting the Al foils tended to destroy them.

Previous workers have shown that the thickness of the oxide layer depends almost entirely on the anodizing voltage and not on the exposure times to acid or base or on other variables. The foils used in this work were made at 148 ± 1 volts. An attempt was made to keep all other variables approximately constant so that any small effects would be reduced even further in importance. The relation between voltage and film thickness appears well established. For example, Harris gives 0.48 $\mu g/cm^2$ per volt or 71.0 $\mu g/cm^2$ for 148 volts.[25] The graphs given by both Walkenhorst and Young give a thickness of about 69.7 $\mu g/cm^2$ at 148 volts.[26,27] Davies et al. quote 0.475 $\mu g/cm^2$ per volt which yields 70.3 $\mu g/cm^2$ for 148 volts.[28] (It should be mentioned that Davies et al. specify that their formula applies only to "preanodized" foils. However, it seems likely that this distinction is necessary only at the low voltages (< 30V) they used and may be neglected here). A simple average of the above thickness values yields 70.2 $\mu g/cm^2$ for the foils used in this work.

Counters and Counting Techniques. The gross alpha radiation of the target and catcher foils was measured using some or all of a series of fourteen 2π ionization chambers designed in this laboratory for detecting fission, alpha and beta activity. Background counting rates were 0.1 to 0.5 cpm. The counting efficiencies of the ionization chambers were approximately equalized by adjusting the amplifier gains so that a thick uranium standard counted nearly equally on all counters. To average out any small efficiency differences, the radiation from the foils was measured by several counters. It was clear from the character of the decay curves that counter differences never exceeded 1%. From counting known standards, counter efficiency was found to be 51 ± 1%.

Energy spectra of the alpha radiation from the foils were measured in two Frisch grid ionization chambers. Signals from these were led through separate preamplifier-amplifier systems and thence via a

routing box into separate quadrants of a 400 channel pulse-height analyzer. The detection efficiencies of the two chambers were identical to within 0.5% and, by comparison with the gross counters, were found to be 46.8 ± 1%. Background, due to electronic noise and chamber contamination, was about the same for the two chambers and was less than 0.001 cpm per channel. Thus background had to be taken into account only for the very lowest counting rates and even then the correction was small. The system was calibrated for energy using a standard consisting of a small amount of Pu^{239} and Am^{241} electroplated on a platinum disk. The alpha energies were taken as 5.15 MeV and 5.48 MeV respectively.[29] Verification that the amplification of the system was linear came from the fact that the well-defined 7.44 MeV peak of the decay product Po^{211} fell on the extrapolation of the line previously determined from the standard peaks.

The same standard sample was used to provide a measure of the resolution of the system. (For purposes of this work "system resolution" will be defined as the width in energy units at half maximum of the 5.15 MeV Pu^{239} peak.) This resolution varied slightly from experiment to experiment, the variations being due chiefly to quality differences in the argon-methane gas mixture used. For a short count, say 10 minutes, the value was usually around 36 keV although runs at 34 keV and 42 keV are also included in the data. For longer counts, say 24 hours, slight electronic drifting produced values of up to 45 keV. These values of the resolution were never realized during foil counting due to the degradation in the alpha energies during escape from the catcher foil; however, quite good separation of most of the alpha peaks in the region of interest was possible. (See Appendix A.)

A. Bombardments of Natural Iridium; Aluminum Catcher Foils

Stacked foils were arranged as in Fig. 2. Such a package, containing two targets in all, was clamped to a water-cooled copper holder and irradiated for about two hours with a beam current of 0.1 to 0.2 μA. An electrometer connected to the copper holder was used to monitor the beam. After bombardment, the foils in the stack were carefully peeled apart and their alpha activities determined on the gross alpha counters. The first counts could generally be made within 30 minutes of the end of the bombardment. The separation of the foils was relatively simple as long as the beam current did not exceed about 0.3 μA. At higher intensities, small areas of fusion often rendered separation difficult or, in some cases, impossible.

The purpose of these experiments was to provide a measurement of the recoil ranges of products derived from compound nucleus reactions. Natural iridium consists of 37.3% Ir^{191} and 62.7% Ir^{193} so that bombardment with O^{16} yields the compound nuclei $[At^{207,209}]^*$. Subsequent decay can lead to the neutron deficient Po and At α emitters. Transfer reactions would of necessity lead to products of lower mass and, particularly, proton number and would produce no nuclides with appreciable α-branching ratios. Thus, measurement of the alpha activity indicates the position of the compound nucleus products in the foil stack. The experimental observations yield the component R of the recoil range along the beam direction. The distribution of these range values, P(R), may be represented by a Gaussian function

$$P(R)dR = \frac{1}{R_m\rho \quad (2\pi)} \exp\left[-\left(\frac{R - R_m}{2^{1/2} R_m\rho}\right)^2\right] dR \qquad (1)$$

where R_m is the average range, ρ is the measured straggling parameter, and $R_m\rho$ is the range straggling.

The experimental results were fitted to Eq. (1) as shown in Fig. 3, where F_t, the fraction of the total activity passing through thickness t, is plotted against t on probability paper. The targets were taken as equivalent to 0.27 W $\mu g/cm^2$ Al where W is the thickness of the iridium in $\mu g/cm^2$.[17] For the target thicknesses used, this was always a very small correction. If the Gaussian function is indeed a good approximation of the activity distribution, the probability plot will be a straight line. This was the case for all the O^{16} irradiations of iridium.

The median range, R_m, is taken simply as the t value for $F_t = 0.5$. The t value for which $F_t = 0.0787$ gives $R_m (1 + \sqrt{2}\rho)$ whence ρ may be obtained. The results of these experiments, along with the results of Ref. 17 for O^{18} on iridium, are presented in Table I. The probable mass of the recoiling species, A_R, is recorded in column 7. A_R was estimated by comparing the half lives of the foil activity with the half lives of known alpha emitters in this region of the periodic table.[9,29] For example, for $E_b = 152.3$ MeV the alpha activity had $t_{1/2} \cong 12$ min; this was attributed to Po^{199} and the probable A_R set at 199. For $E_b = 102.9$ the activity had $t_{1/2} \cong 8$ min initially, but this faded to a 50 min tail. The recoils were assumed to be Po^{200} and Po^{202} and the probable A_R was set at 201. As might be expected, the A_R's from this work were usually two units less than those derived from the O^{18} bombardments at similar E_b's.

If the assumption is made that the recoil velocity is not altered by the decay of the compound nucleus, the recoil energy of the final product, E_{TMT}, is given by

$$E_{TMT} = E_b A_b A_R / (A_b + A_\tau)^2 \qquad (2)$$

where A denotes mass number, b the bombarding particle, R the recoil atom and τ the target. Values of E_{TMT} calculated in this way are listed in column 8, Table I. In Fig. 4 are plotted some of the data from Ref. 17 along with some values from this work. It is seen that agreement is excellent.

B. Bombardments of Natural Iridium; Aluminum Oxide Catcher Foils

The target-catcher stack was suspended in the Hilac beam with the device shown in Fig. 5. The same targets used for the Al leaf experiments were used here; they were mounted on stainless steel rings in sandwiches similar to those used for the catcher foils. After insertion of the target foil followed by sufficient catchers to collect the α activity, the trough was filled with empty rings so that the foils were packed as closely together as possible. This placed them about 0.022 in. apart when 0.010 in. rings were used and about 0.038 in. apart for 0.018 in. rings. The surfaces of the rings were scored to ensure that the spaced between the foils could be evacuated easily without rupturing the foils.

A schematic diagram of the bombardment arrangement is shown in Fig. 6. The foil holder was secured to the second collimator in such a way that a quarter turn released the entire holder. This fact, along with the ease of separation of the foil packages, allowed counting to begin 15 to 20 min after the end of the bombardment. The Al_2O_3 foils mounted in this manner could withstand a beam flux of over 10^{-6} A, but since sufficient activity could be obtained from less than half this value, beams of 0.3 to 0.4 μA were generally used.

The purpose of these experiments was to provide an empirical relation between the relative stopping powers of Al and Al_2O_3 for recoils of At and Po. Therefore, the data processing for the Al_2O_3 runs was very similar to that from the Al leaf runs described in Section A above. Two minor differences occurred. Because the Al_2O_3 foils were thinner, a few pulse height analyses of the α activity were possible. These provided confirmation of the A_R values. Also, the probability plots generally showed somewhat less scatter for Al_2O_3 foils than for Al leaf. This suggests that the difference in thickness among the Al_2O_3 foils used was less than the error in measurement of the Al leaf and might also reflect an improvement in foil homogeniety with Al_2O_3.

The results are collected in Table I, and a range vs E_{TMT} plot for Al_2O_3 has been included in Fig. 4. It is seen that at a given recoil energy, the range in mg/cm^2 of Al_2O_3 is about 7 to 11% greater than that in Al. The values of the straggling parameter, ρ, show no particular trend with energy; this is not unlike the behavior in Al. The ρ values for Al_2O_3 do seem to be consistently 20% lower than those for Al.

The significance of these differences is discussed in Section III.

C. Bombardments of Bi^{209} and Pb^{208}; Aluminum Oxide Catcher Foils

Separated Pb^{208} was obtained from the Isotopes Division, Oak Ridge National Laboratories. The composition in atomic percent was given as: Pb^{208}—97.98; Pb^{206}—1.15; Pb^{207}—0.82; Pb^{204}—0.07. Sufficient Po^{210} was present to have produced about 2.2 cpm of α activity from 138 day Po^{210}.

The arrangement of target and catcher foils for these experiments was similar to that for the oxygen on iridium bombardments described in Section B, above. Irradiations lasted three to nine hours and beam currents were 0.1 to 0.3 μA After bombardment, the radiation from the foils was measured once on the gross alpha counters to locate the activity. The pertinent foils were then cycled continually through the two grid chambers for energy analysis. Counting times were increased gradually from 4 min in the early stages to 3 hrs three to four days after bombardment. The long-lived activities were determined by thousand minute (or more) counts taken at approximately monthly intervals. The decay of all samples was followed for at least four months; in some cases, determinations extended to eighteen months.

The pulse-height spectra from these runs consisted of 3 to 9 peaks, most of which were well separated. The peaks were assigned to specific nuclides by comparing the α energies and half lives with known α emitters. Table II lists these assignments along with energies and

half lives as determined here and in other work. Details concerning the general analysis and also the peculiarities of each product are described in Appendix A. Suffice it here to say that the activities at the end of bombardment for each product in each catcher foil were obtained in the usual way by extrapolating the decay curves back to the appropriate time. Since the catcher foils were all of the same thickness, these initial activities may be used to represent the projected range distributions.

With Bi targets, exposures to O^{16} were made at energies of 163 (two), 152, 123, 110, 85, and 76 MeV. With Pb^{208} targets, O^{16} energies were 163 and 123 MeV. As was implied in the introduction, the range distributions obtained were extremely complex; except for a few instances, all were definitely non-Gaussian. Since the shapes vary so widely it would be difficult, tedious and probably not highly informative to attempt to describe each result. Therefore, the actual range distributions are given in Table III. A few selected examples are shown in Figs. 7 through 10.

In Table III, the numbers given under the "Activities" heading correspond approximately (except for Rn^{211} and At^{211}) to the initial counting rates in cpm. In an attempt to reduce the data to more easily assimilable form, three projected ranges were determined for each distribution. All are given in units of one Al_2O_3 foil thickness (70.2 $\mu g/cm^2$) and include the correction for target thickness used by Alexander and Winsberg, i.e., $\Delta R_\tau = \frac{1}{2}(0.535)W$ where ΔR_τ is the correction, and W is the target in appropriate units. This correction should introduce only a very small error. (The distributions as given in Table III have been rounded off somewhat from those used for calculating the average and median ranges; the persevering reader who attempts to reproduce the range calculations may thus find small discrepancies.) R_m is the median range and is defined so that one-half the particles have range greater than R_m. It was obtained from a probability plot (see Fig. 3). R_a is the average range given by

$$R_a = \sum_i f_i \left(t + \tfrac{1}{2} t_i\right)$$

where f_i is the fraction of the total activity found in a given foil, t is the total thickness of the stack up to the given foil and t_i is the thickness of the given foil. R_p is the peak range. It was obtained by reading off the range at the peak of the range distribution from plots such as those in Figs. 7 to 10.

For distributions that are asymmetrical due to a long range tail, $R_p < R_m < R_a$. Conversely, a short range tail would make $R_a < R_m < R_p$. A comparison of R_p, R_m and R_a thus gives a crude estimate of the degree of asymmetry. It should be noted that both R_m and R_a are somewhat sensitive to the experimental conditions; both increase as the initial activities increase or as the number of counters available increase, although R_a is affected more. (The reason for this is that measurements on the long-range side of the peak can be pursued to longer ranges under these conditions. For example, for Run II (see Table III), a second grid chamber had been added to the one used in Run I. Also, a faster analyser print-out system was available. Thus, even though the bombarding energies and activities were about the same, more foils could be counted in Run II. Corresponding R_m and R_a values are generally somewhat higher in Run II.)

The ranges expected for an At^{211} product from a compound nucleus reaction (R_{TMT}) are also given in Table III. These were estimated using Eq. (2), and the range-energy curve for At in Al_2O_3 determined in the O^{16} + Ir experiments. Perhaps the most outstanding feature of the range distributions is that, while at high energies they peak at values roughly $1/4 R_{TMT}$, the peaks tend to increase in range as the bombarding energy decreases. This is particularly true in the region from 123 MeV to 76 MeV. In fact, for the two Bi runs at 85 and 76 MeV the distributions peak well beyond that range expected for the total momentum transfer reaction. Discussion of these interesting phenomena, which were first

observed by Alexander and Winsberg, will be left until the angular distribution data have been introduced in the next section.[16] To allay the reader's apprehension that the laws of conservation of energy and momentum might somehow have been violated, it should be pointed out that ranges beyond the compound nucleus range are possible if particles are emitted preferentially in the backward direction.

Rough estimates for the total cross sections for each product are also listed in Table III. With both the low melting metals Bi and Pb, some difficulty was experienced with loss of target material due to overheating in the beam. The ever-present beam-spot discoloration make it difficult to judge such a loss. It was probably very small for the low energy bombardments, but an accidentally high focusing of the only slightly degraded beam "burned" areas of the target in some high energy runs. Another difficulty lay in the correction for decay-during-bombardment. The Hilac crew made a valiant effort to keep the beam level constant throughout the 3 to 9 hour bombardment periods but the inevitable electronic drifting and occasional shutdowns prevented this. Only the cross sections for the short lived Fr^{212}, Rn^{212} and to a much lesser extent, Rn^{210} would be appreciably affected by this source of error. Range distributions should be unchanged.

D. Bombardments of Bi^{209} and Pb^{208}; Angular Distribution Experiments

Because of the low activities encountered, the angular distribution measurements were somewhat crude. Fig. 11 shows the apparatus used in these bombardments. The target could be placed at various angles to the beam; usually 60° was chosen. The catching strip covered from about 9° to 96° and was generally cut into ten sections of around 8.7° each. With the geometries involved, this meant that each catcher subtended about 0.03 steradians. In the first experiments performed, ordinary household Al foil was used for the catcher strip, and the

gross α decay curves were measured. From these it was clear that the α activity had definitely different compositions at various angles. Therefore, in spite of the difficulties presented by the low activities produced, an attempt was made to obtain range and composition data for each 8.7° segment.

Four strips of Al leaf were placed on top of the thick Al strip and the assembly was clamped in the holder. After bombardment, the foils could be appropriately cut, separated and counted on the gross α counters. The composition of the activity in each foil was then deduced from analysis of the decay curve. Usually pulse-height analyses were not attempted; not only was peak resolution poor because of the thick foils, but counting rates were so low that it was impossible with only two grid chambers to obtain adequate counting statistics on all of the 30 to 40 foils with appreciable activity produced in each experiment.

Without energy analyses it was not possible to identify each of the 7 to 9 components known to be present from the previous experiments. By the time the foils were cut and mounted, the short-lived Fr^{212} and Rn^{212} had decayed too far to be quantitatively determined. Qualitatively, the short-lived components were strongly peaked forward. If a 14.6 hr. component was present in the decay curve, the curve was fitted graphically at long time to the "Master Curve for Rn^{211}" as given in Fig. 12. The difference between the master curve and the experimental curve was resolved into two components of 2.42 hrs. and 7.21 hrs. and these were assigned to Rn^{212} and At^{211} respectively. About one month after the bombardment, and again at about 3 months, counts were taken with the pulse-height analysis system and the activity between 5.0 and 5.3 MeV was fitted to a 138.4 day half-life; this was assigned to Po^{210}. The above method of analysis ingores Po^{206}, if present. At^{209} would contribute to the "7.21 hr. component", but from the previous experiments this contribution is estimated to be less than 10%. Similarly any Po^{208} present could contribute to the "Po^{210}" component to an extent less than 10% of the total. As before "Po^{210} must include (Bi^{210} + Po^{210} + At^{210}).

The activity distributions of the four extracted components are shown in Figs. 13 through 16. These plots deserve some explanation. The activities have been given arbitrary units to separate the curves in the figures. The points are plotted at the mid-points of the 8.7° angular sections. For some of the larger angles it was not always possible to extract a 2.42 hr. component; that is, after subtraction of the Rn^{211} master curve, the remainder could be fitted by a 7.21 hr. component alone. Since the counting rates of the foils were so low, however, statistics were poor and there was the possibility that some Rn^{210} was indeed present. In the foils at small angles the ratio Rn^{210}/Rn^{211} was essentially constant for a given experiment. This ratio was therefore used to estimate the possible Rn^{210} contribution in the foils where it was not possible to separate it. These points are represented in Figs. 13 to 16 by open triangles and are attached to the other Rn^{210} points by a dashed line. Corrected activities were calculated for At^{211} in these foils by subtracting the calculated Rn^{210} activities. The corrected At^{211} points are indicated by closed triangles, and they too are joined to the other At^{211} points with a dashed line. The two curves for At^{211} thus represent a minimum and maximum At^{211} distribution.

The purpose of all this was to show that the rather prominent peaking observed in the At^{211} curve was indeed real, and was not due merely to some accident of the analysis.

The range distributions obtained from these experiments were not extremely accurate. (See Appendix C for a fuller discussion of the errors involved.) In an effort to extract useful information the data were processed in the following way. The small foil stack at each angular segment was treated by the probability plot method described earlier. Because of the thickness of the Al leaf (174 ± 16 $\mu g/cm^2$) and the generally small ranges (130 to 330 $\mu g/cm^2$) the activity tended to be concentrated in the first two foils and rarely extended as far as the 5th foil to any appreciable extent. The paucity of the

points, as well as their scatter due to poor counting statistics, made analysis of the curve on probability paper somewhat difficult. However, it appeared that the distributions were again non-Gaussian, containing a long-range tail. The median ranges at each angle, R_θ, were read off and are listed in Table IV. The correction for target thickness was made (the variation with angle was considered), but of course the activity lodged in the target which, had it escaped, would have contributed to a given angular catcher was unknown. From the runs with Al_2O_3 catchers, this error could be estimated at 5 to 10% for the At and Po ranges and ~1% for the Rn; that is, the measured ranges are too large by these amounts. Overall, errors could be as high as 35% for some measurements.

Also given in Table IV is the average projected range, $\overline{R}_{proj}$, defined by

$$\overline{R}_{proj} = \frac{\Sigma_i \; R_{\theta_i} \; \cos\theta_i \; A_i}{\Sigma_i \; A_i}$$

where R_{θ_i} is the median range at angle θ_i and A_i is the total activity found in the entire foil stack at θ_i (integrated over azimuthal angles). The $\overline{R}_{proj}$ values have been changed to units of "Al_2O_3 foils" by the transformation 1 $\mu g/cm^2$ Al = 1.06/70.2 Al_2O_3 foils where 1.06 is the ratio of the ranges of At, Po in Al_2O_3 and Al (for low ranges) obtained from the Ir experiments and 70.2 is the thickness of an Al_2O_3 foil in $\mu g/cm^2$. $\overline{R}_{proj}$ would be expected to correspond approximately to R_m as measured in the stacked Al_2O_3 catcher experiments. In 9 of the 16 cases, agreement is better than 8%; in only one case is the difference more than 16%. Considering the statistical errors, this is quite reasonable agreement, and suggests that the method of analysis has been successful.

In order to determine the recoil energies of the At and Po products which were peaking at such large lab angles, an average range at the position of the peak was obtained; that is,

$$R_{\theta_p} = \frac{\Sigma_j R_{\theta j} A_j}{\Sigma_j A_j}$$

was determined, where the sum was taken only over the 3 or 4 points in the peak. Since the range energy curve for At, Po in Al is known, the recoil energies of these products can then be read off the graph (Fig. 4). The R_{θ_p} values obtained, with their associated recoil energies, are also given in Table IV. Use of the recoil energies to help define the mechanism is included in the next section.

III. DISCUSSION

In this section, we examine all the data from the different types of experiments and attempt to produce a description of the reactions studied. As was implied earlier, the situation is so complex that a full description will not be possible. Many general characteristics and a few specifics can, however, be given. Although the experiments were all rather strongly interrelated, for ease of discussion a division will be made between those concerned chiefly with the stopping of heavy recoils, and those concerned chiefly with nuclear reactions.

A. Range-Energy Curves for At, Po Recoils

The passage of heavy charged particles through matter is now being studied by a variety of methods.[30] Theories and some semi-empirical considerations can serve to provide fairly accurate range-energy curves for many ions in many stopping materials, particularly for very high or very low velocities. For the intermediate velocities, however, where both electronic and atomic stopping are important, the best way to obtain a particular range-energy curve is by experiment with the ion and stopping material required. Unfortunately, such empirical studies are not always possible, let alone convenient. For this work, however, a close approximation to the ideal situation was at hand. Required was a range-energy curve in some convenient stopper for Po, At, and Rn products of mass roughly 208 to 212; already available was an empirical range-energy curve for At and Po of mass 199 to 207 in Al leaf. The error introduced by applying a range-energy curve for ${}_{84}Po^{199}$ to a recoil atom ${}_{86}Rn^{212}$ is very small. As it happened, Al_2O_3 was a more convenient catching material, so experiments were performed with (a) Al leaf catchers to consolidate the old data for Al and (b) Al_2O_3 catchers to establish a similar range-energy curve for Al_2O_3. Since

the (a) and (b) experiments were identical except for catcher foil, a direct comparison of the ranges in Al and Al_2O_3 was also obtained.

As we have seen (Fig. 4), the range-energy curve for At, Po in Al leaf is well defined by the combined data points from this work and Ref. 17. Ranges in mg/cm^2 of Al_2O_3 are about 7% greater than for Al at a recoil energy of 6 MeV and about 11% greater at 12 MeV. For this energy region (recoil ranges from about 450 to 800 $\mu g/cm^2$ Al_2O_3) the range-energy relationship is expected to be very accurate. Actual recoil ranges in the Bi and Pb experiments, however, varied from about 100 to 1100 $\mu g/cm^2$ Al_2O_3. As seen in Fig. 4, extrapolation to low ranges cannot lead to a large error. Extrapolation to high ranges can be guided by the Tb^{149}-in-Al line, but as the shaded area indicates, there can be some question about the proper course the extrapolation should take. Therefore a different method of extrapolation for high ranges was sought.

Lindhard, Scharff and Schiøtt(LSS) have developed a theoretical treatment for the stopping of heavy ions.[31] They attempt to derive universal range-energy curves by changing from R-E coordinates to ρ_L-ϵ coordinates where

$$\rho_L = R \frac{4\pi (0.8853)^2 a_o^2 N_2 A_1 A_2}{(Z_1^{2/3} + Z_2^{2/3})(A_1 + A_2)^2} \tag{1}$$

and

$$\epsilon = E_1 \frac{(0.8853) a_o A_2}{Z_1 Z_2 e^2 (Z_1^{2/3} + Z_2^{2/3})^{1/2} (A_1 + A_2)} \tag{2}$$

Here, the subscripts 1 and 2 refer to the ion and stopper respectively, N is the atomic density and a_o the Bohr radius ($\hbar^2/me^2$). Thus, ρ_L and ϵ are dimensionless measurements of range and energy. In effect, the factors multiplying the R and E values serve to "correct" these for A and Z dependence. In these coordinates, then, LSS take the total stopping power to be composed of contributions from both the "nuclear" or atomic stopping as well as electronic stopping. That is,

$$\left(\frac{d\epsilon}{d\rho_L}\right)_{Tot} = \left(\frac{d\epsilon}{d\rho_L}\right)_n + \left(\frac{d\epsilon}{d\rho_L}\right)_e$$

where $$\left(\frac{d\epsilon}{d\rho_L}\right)_e = k\epsilon^{1/2}$$

and $$k = \frac{(0.0793)\, Z_1^{2/3}\, Z_2^{1/2}\, (A_1 + A_2)^{3/2}}{(Z_1^{2/3} + Z_2^{2/3})^{3/4}\, A_1^{3/2}\, A_2^{1/2}}$$

The nuclear stopping is derived from a statistical (Thomas-Fermi) treatment of atomic collisions.

In Fig. 17 the dashed lines represent the paths of constant k as derived from the graphs given by LSS. The curve for k = 0 represents pure nuclear stopping. It is seen that as ϵ increases and electronic stopping becomes more and more important, the curves for finite k fall away from the k = 0 curve; i.e., for a given energy the range is lower due to the electronic stopping contribution. Many of the data points from Fig. 4 are also plotted in Fig. 17. As is seen, k is an extremely slowly varying function of Z and A in this region of the periodic table—all the interactions listed have the same k value. Clearly, the transformation to ρ_L-ϵ coordinates has succeeded in bringing the Al stopping data together on the same curve. However, this curve does not follow the theoretical k = 0.11 line but quite definitely crosses it. This behavior is similar to that observed by Gilat and Alexander for the stopping of Dy in various gases and by Kaplan and Fink for Sm in Al.[19,32] With the assumption that this type of behavior is typical, we can now use the Al curve to guide the extrapolation of the Al_2O_3 curve.

In the region of ϵ where data points for At in Al_2O_3 are available, the curves for Al and Al_2O_3 are essentially parallel. This characteristic was assumed to hold at higher ϵ and the Al_2O_3 line

was extrapolated as drawn, parallel to the Al curve. It should be noted that a range of 1100 $\mu g/cm^2$ Al_2O_3 corresponds to a $\rho_L \approx 30$ so that the extrapolation was not extreme and is expected to be accurate to about ± 5%.

It is interesting to digress briefly to discuss possible reasons why the Al_2O_3 curve is so far removed from the Al curve in spite of the similarity in k values. One possibility lies in the difficulty in deciding what to use in Eq. (3) and (4) for Z_2 and A_2 of Al_2O_3. The values actually used were the simple averages $Z_2 = 10$, $A_2 = 20.4$. Better values may exist; however, it seems reasonable that $8 < Z_{Al_2O_3} < 13$ and $16 < A_{Al_2O_3} < 27$ and whatever method of "averaging" is chosen, the results cannot differ widely from the values used here. A small change in, for example, A_2, causes only small changes in the ρ_L-factor and the ϵ-factor and both these changes are in the same direction. Thus, although a given data point is moved slightly by assuming different Z_2 and A_2 the line drawn through the points retains essentially the same position.

The main reason, of course, for the difference between the Al and Al_2O_3 curves on the ρ_L-ϵ plot (Fig. 17) is the fact that the curves lie so far apart on the R-E plot (Fig. 4); that is, addition of O atoms to Al increases the range (in mg/cm^2) by 7 to 11%. This result appears to be in opposition to previous experiments with ions of mass 11 to 19 and energies of 2 to 10 MeV/amu which showed O_2 gas to be a better stopper than Al.[24,33] Also, Piercy et al. compared Al and Al_2O_3 as stoppers for Kr^{85} ions of 0.47 keV/amu and found Al_2O_3 to be more effective.[34] Both of these results, however, were for ion velocities quite different from those in the present work, where the recoil energies were 30 to 60 keV/amu. Working in the energy region 40 to 100 keV/amu, Gilat and Alexander found that ranges of $Dy^{149,150,151}$ in N_2 were slightly greater than the ranges of Tb^{149} in Al (Fig. 4).[32] Ranges in Ne were about 30% greater than the Al values. If the range in O_2 lies

between the values for N_2 and Ne, we see that qualitatively at least, the effect found in the present work is in the right direction and is of about the correct magnitude.

The comparison can be made semi-quantitatively as follows. If we assume that the stopping cross sections due to Al and O atoms are proportional to the same power of the energy, we can use the formula given by LSS for the range in mixtures,[31]

$$R_{Al_2O_3} = \frac{R_{Al}\, R_O}{x_{Al} R_O + x_O R_{Al}} \tag{5}$$

where R_i is the recoil range in substance i and x_i is the relative abundance of component i in the mixture.[35] Table V shows Dy ranges in N_2 and Ne at two appropriate recoil energies, and ranges in O_2 obtained by linear interpolation. Tb ranges in Al at the same energies were read from Fig. 4. The range in Al_2O_3 predicted from Eq. (5) is seen to be 5% greater than the range in Al. This is quite close to the experimental 7 to 11% obtained for At, Po recoils—errors in determining the ranges could easily account for the difference. The following not necessarily independent considerations might affect applicability of Eq. (5) in this case, but no attempt will be made here to assess their influence. (a) The stopping power of oxygen atoms in the gas may be different from that of oxygen in the solid Al_2O_3. (b) Al is a good conductor while Al_2O_3 is not. (c) The interpolation for R_O may be in error, particularly if shell effects are important at these low values of Z. (d) The chemical bonding in Al_2O_3 may affect electron densities so as to alter the stopping powers of Al and O from their elemental values.

Let us now briefly consider the straggling information obtained in these experiments. The data extend over too small an energy region for detailed analysis to be justified; however a few qualitative remarks may be made. As has been mentioned, no definite trend of the ρ values with changing recoil energy was observed in either Al or

Al_2O_3. The ρ's are consistently lower in Al_2O_3. The measured straggling parameter results from a number of effects which combine approximately as the squares. That is,

$$\rho^2 \approx \rho_s^2 + \rho_f^2 + \rho_n^2 + \rho_w^2 \tag{6}$$

where ρ_s is the straggling due to the stopping process, ρ_f to the foil inhomogeneities, ρ_n to the velocity distribution resulting from the nuclear reaction, and ρ_w to the target thickness.

We will now use Eq. (6) to attempt to locate the source of the difference in measured straggling between Al and Al_2O_3. The relative magnitude of ρ_w is very small and may be neglected here. For ρ_n we will use the value 0.1 which should be correct to within 10%.[36] (A 10% error in ρ_n would have little effect on the conclusions reached below.) If "typical" measured ρ values of 0.25 for Al and 0.20 for Al_2O_3 (Table I) are used, the following relation results from Eq. (6) in a straightforward way:

$$\frac{(\rho_s^2 + \rho_f^2)_{Al}}{(\rho_s^2 + \rho_f^2)_{Al_2O_3}} \approx 1.7 \tag{7}$$

If foil inhomogeneities contribute little to the straggling, the ρ_f's may be disregarded and Eq. (7) reduces to

$$\frac{(\rho_s^2)_{Al}}{(\rho_s^2)_{Al_2O_3}} \approx 1.7$$

This is a substantially larger ratio than that predicted by the LSS theory.[31] Qualitatively, this suggests that the ρ_f's <u>cannot</u> be ignored and that $(\rho_f)_{Al} > (\rho_f)_{Al_2O_3}$. As was mentioned earlier, the

smaller scatter on the probability plots for Al_2O_3 as compared to similar plots for Al also led to the suspicion that Al leaf inhomogeneities were not negligible.

B. Nuclear Reactions

The complicated data from the range and angular distribution experiments with Bi and Pb targets have been presented with relatively few guiding comments. Such comments were postponed until this point so that the entire body of data would be available for the extraction of information.

Let us consider first the Bi bombardments. For bombarding energies greater than about 1.3 E_{Coul} (where E_{Coul} is the Coulomb barrier energy for r_o = 1.5 fermis), several products are observed. In the region $E_b \approx 1.3\ E_{Coul}$, however, the production of Po^{208}, At^{209} and the three radon isotopes decreases rapidly with decreasing energy. In the low energy runs at and below the barrier, only At^{211} and Po^{210} are detected. The general features of momentum transfer are similar to those indicated by the less detailed experiments of Alexander and Winsberg: fractional momentum transfer increases with decreasing bombardment energy.[17] At high bombarding energies (about twice the Coulomb barrier), the projected range distributions peak at about one-quarter the range of the compound nucleus, R_{TMT} (see Table III). As E_b decreases, the R_p values remain approximately constant but, of course, R_{TMT} is decreasing; hence, at 1-1/2 times the barrier, the range distributions peak at about 1/3 R_{TMT}. Further decrease in E_b leads to a more rapid increase in R_p; at E_b about 1-1/3 times the barrier, the R_p's are nearly half the full momentum transfer range. Just above the Coulomb barrier, the range distributions for Po^{210} and At^{211} peak at more than 1-1/2 times R_{TMT}. At E_b(c.m.) = 0.93 E_{Coul}, the products are found three times deeper in the foil stack than the point reached by the compound nucleus.

Let us examine this low energy experiment in some detail. For both At^{211} and Po^{210} the range distributions are quite symmetrical as shown by (a) the approximate linearity of the probability plots and (b) the similar values for R_p, R_m and R_a. (The fact that only 20 foils were used in the experiment meant that the last tip of the high-range tail was lost. This undoubtedly contributed to the slightly low R_a values given in Table III). Taking 14.4 and 15.9 foils as the ranges of At^{211} and Po^{210} leads to recoil energies of 15.8 and 17.9 MeV respectively. E_{TMT} for At^{211} is 5.14 MeV for this bombarding energy. Let us suppose that the excess energy is given to the recoil in the following way. Let O^{16} approach the Bi^{209} with a very small impact parameter. At the distance of closest approach, we have the following situation. The O^{16} and the Bi^{209} are nearly at rest with respect to each other, but their center of mass is moving with the initial beam momentum. Now let an α particle transfer into the Bi^{209} to form $[At^{213}]^*$ and let the C_{12} residue roll back down the barrier and be ejected in a backward direction. The $[At^{213}]^*$ in this way can acquire of the order of 1.75 times the momentum of the projectile and a recoil energy $(1.75)^2 E_{TMT} \approx 3 E_{TMT}$. Evaporation of two neutrons from the $[At^{213}]^*$ would yield At^{211}. A (3n) or (p,2n) emission would lead to the Po^{210} observed.

A mechanism of this sort seems quite promising, but let us look into the energetics more closely. (The Q values and masses used in the following were estimated using Ref. 9, and are listed in Table VI.) For production of At^{211} we have

$$Bi^{209} + O^{16} \longrightarrow [At^{213}]^* + C^{12} + Q_1$$

where $Q_1 = -16.6$ MeV and E^* must be greater than 10.9 MeV to allow evaporation of 2 neutrons. In the lab system, conservation of momentum and energy requires, for zero impact parameter, that

$$P_O = P_{At} - P_C \qquad (8)$$

and

$$E_0 = E_{At} + E_C + E^* - Q \qquad (9)$$

From E_0 = 75.8 MeV, E_{At} = 15.8 MeV and Eq. (8) we get E_C = 44.5 MeV. Substituting this into (9) yields

$$75.8 = 15.8 + 44.5 + E^* + 16.6$$

$$E^* = -1.1 \text{ MeV}$$

Clearly there is not sufficient energy present to produce an At^{213} recoil with 15.8 MeV kinetic energy, let alone one with over 10.9 MeV excitation energy as well. If 2n evaporation is impossible, obviously 3n or p2n evaporations cannot occur either. Since we considered the case of maximum energy transfer (i.e., zero impact parameter), we must conclude that α transfer is not the source of the At^{211} and Po^{210} observed. (Actually, since neutrons are unlikely to come off with near-zero kinetic energy, the E* requirement should have been set even higher. Moreover, the C^{12} might also carry off some excitation energy. Inclusion of both of these effects would make the conclusions of the above argument even more definite. For simplicity, however, such effects were not considered.)

If C^{12} "emission" provides insufficient momentum transfer, it is clear that a heavier particle must be ejected from the reaction site. Suppose At^{211} results from the 2p transfer reaction

$$Bi^{209} + O^{16} \longrightarrow (At^{211})^* + C^{14} + Q_2 \quad .$$

Here Q_2 = -14.4 MeV and $E^* \lesssim 7.6$ MeV to prevent neutron evaporation. Proceeding as above, $E_{C^{14}}$ = 37.5 MeV, whence E* = 8.1 MeV. Now the reaction is not only energetically possible, but in some cases a neutron may be evaporated, and Po^{210} may result from the At^{210} electron capture. (This effect must be small. The probability for emission of a neutron

with only ~0.5 MeV kinetic energy is very low. Moreover, the peak of the Po^{210} distribution is 10% deeper in the foil stack, suggesting that most Po^{210} comes from a different mechanism.)

Other potential reactions for production of Po^{210} are listed in Table VII. The numbers in the 7th column are again simply the appropriate neutron binding energies. The last column contains E* calculated using equations similar to Eqs. (8) and (9) with E_{Po} = 17.9 MeV. Clearly production of the long-range Po recoils by two-nucleon transfer is not energetically possible, though both of the single-nucleon transfer mechanisms could yield the observed Po^{210}. The recoil data provides no basis for choice between n or p transfer, since the momentum transferred is the same in each case. However the decay curves can be helpful; they show no evidence of growth of Po^{210} from the 5 day Bi^{210} so that an upper limit of 20% of the observed Po^{210} could have come from n transfer.

It must be emphasized that these experiments are sensitive only to α emitters so that a transfer or compound nucleus mechanism which does not yield an α-active product cannot be detected. Thus, these experiments do not show, for example, that α transfer does not occur, but only that α transfer cannot lead to the At^{211} and Po^{210} produced. The sum of the cross sections for At^{211} and Po^{210} is ~16 mb which is about equal to that obtained for the total reaction cross section by interpolation from Thomas' tables (~12 mb).[11] It is not clear, however, that this comparison is meaningful, as the tables would be expected to be least accurate in this barrier region. It is interesting that the cross section for 2p transfer (~5 mb) is about half that for single p transfer (~11 mb). This is a much higher ratio than would be expected from a tunneling mechanism. Nevertheless the conclusions seem inescapable from the above consideration of the energetics. (The effects of energy spread in the beam and non-zero impact parameters are considered in Appendix C, page 83, and are shown not to change these conclusions).

As the bombarding energy is increased, the collisions with low impact parameters should contribute more and more towards compound nucleus formation. The p and 2p transfer reactions will occur at larger impact parameters; the C^{14} and N^{15} will still be emitted in a backward direction but no longer at near-zero angles. The momentum transferred will be reduced and the At and Po recoils will also come off at an angle to the beam. We could expect, then, that the projected recoil range (as measured in a stacked foil experiment) should fall off rather sharply with an increase in bombarding energy. This is exactly what is observed. At E_b = 85.2 MeV [E_b(c.m.) = 1.05 E_{Coul}], the range for At^{211} recoils is about 9.5 foils, or $E_{At^{211}proj} \approx 9.6$ MeV $\approx 1.7\ E_{TMT}$. The results of Alexander and Winsberg at E_b(c.m.)/$E_{Coul} \approx 1.05$ to 1.20 show a steady decrease of E_{At}/E_{TMT} from about 1.4 to 0.9. (See Fig. 5 of Ref. 16).

Proceeding to the higher energy bombardments, we note the appearance, at $E_b \approx 1.3\ E_{Coul}$, of several new products. These products may be the result of new transfer mechanisms which are becoming possible with the increase in energy. On the other hand, they may be the result of peculiarities of the de-excitation processes such that transfer mechanisms which have been occurring all along now begin to contribute toward the α emitters detected. Consider the three Rn isotopes. For the runs with bombarding energy near the barrier (Runs VI and VII, Table III), they were not detected ($\sigma \lesssim 0.1$ mb). For Run V, at E_b = 110 MeV, only Rn^{212} was detected, the cross section being about 3 mb ($\sigma_{Rn^{211}} \lesssim 0.5$ mb; $\sigma_{Rn^{210}} \lesssim 0.1$ mb). At E_b = 123 MeV all three were present, with $\sigma_{Rn^{212}} \approx 12$ mb, $\sigma_{Rn^{211}} \approx 7$ mb, and $\sigma_{Rn^{210}} \approx 1$ mb. For E_b = 150 to 160 MeV, cross sections for the three isotopes are about the same. In summary, increasing bombarding energy causes Rn^{212} to appear first, followed by Rn^{211} and then Rn^{210}.

One explanation for this behavior is that 3p transfer, which produces Rn^{212} directly, has just begun to occur. As the energy is increased the excitation of the Rn^{212} produced increases until the

possibility of neutron evaporation develops. Loss of one neutron, of course, yields Rn^{211}. With further increase in energy, two neutrons may be lost to produce Rn^{210}. The observed order of appearance of the three isotopes with increasing energy is consistent with the above mechanism.

Alternatively, let us consider the transfer of two α particles by the reaction

$$Bi^{209} + O^{16} \longrightarrow [Fr^{217}]^* + 2\alpha + Q_4$$

Here, $Q_4 = -32.3$ MeV. Such a reaction is thus energetically possible at low bombarding energies—whether the reaction actually occurs with appreciable probability depends on details, as yet unknown, of transfer processes. It seems reasonable to assume, however, that if Fr^{217} is indeed produced, its excitation energy will increase with increasing bombarding energy. If this excitation is sufficient to evaporate only one to four nucleons, $Rn^{210,211,212}$ cannot result (see Fig. 18). If an increased E_b leads to an excitation energy sufficient for a p4n evaporation, however, Rn^{212} is the product. Further increases in energy would yield first Rn^{211} (from p5n), and then Rn^{210} (from p6n). Thus, we see that the observed order of appearance of the Rn isotopes is consistent with this mechanism also.

In fact, even a cursory examination of Fig. 18 suggests a number of transfer mechanisms which might be equally consistent with the experimental results. Since we lack knowledge of the details of the transfer processes, the present data cannot provide sufficient information that a choice may be made among these many mechanisms.

It is possible, however, to use the data to guide a few remarks about the general features of transfer reactions. For instance, it is interesting to try to determine what fraction of all transfer processes yield products detected in this work. It will be recalled, as was mentioned in the introduction, that PMT reactions of O^{16} and Bi

do not lead to fission.[13] An estimate of the fraction of the total cross section available for all transfer reactions may be obtained as follows. Britt and Quinton measured the total fission cross section for the C^{12} + Bi reaction at energies from 1.2 to 2.1 times the barrier.[15] In this region they found their results to be well reproduced by the relation $\sigma_f = 0.65\ \sigma_T$ where σ_f is the measured fission cross section and σ_T is the total reaction cross section due to Thomas. For the O^{16} + Bi reaction, the relation was $\sigma_f = 0.72\ \sigma_T$ at $E_b = 168$ MeV, the only point measured. If the factor 0.72 holds at other energies, we can approximate the non-fission interactions as comprising about 28% of the total reaction cross section. Fig. 19 shows σ_T as interpolated from Thomas' tables along with a curve for $0.28\ \sigma_T = (\sigma_T - \sigma_f)$. The sum of the cross sections for all α emitters measured in this work are also plotted. At all energies except those at the barrier, the α-active products make up less than half the non-fission cross section.

An estimate of the cross section for certain undetected nuclides may be obtained by simple interpolations and extrapolations among the values measured. For example, $\sigma_{At^{210}}$ may be assumed to lie between $\sigma_{At^{209}}$ and $\sigma_{At^{211}}$, or $\sigma_{Po^{209}}$ between $\sigma_{Po^{208}}$ and $\sigma_{Po^{210}}$. Also, $\sigma_{Rn^{209}}$ may be obtained from the "trend" established by the three Rn cross sections measured. Addition of such estimated values to the measured cross sections raises the points in Fig. 19 so that they comprise from ~80 to ~100% of the non-fission cross section. It is not possible to say whether this remaining difference is real—that is, whether there are undetected transfer reactions—or whether the difference is due to a combination of errors in (a) the measured cross sections, (b) the σ_T curve, and (c) the assumption that the $\sigma_f = 0.72\ \sigma_T$ relation holds over all E_b. The above discussion also (implicitly) assumes that all TMT reactions lead to fission. It does seem safe to say that information about most of the PMT reactions is obtained from measurements of the α emitters with convenient half lives detected here.

From the above discussion, from consideration of Fig. 18, and from complexities observed in the range and angular distributions, it seems clear that at least some of the products are being produced by more than one mechanism. It seemed reasonable, however, that the pronounced angular peaking for both At^{211} and Po^{210} (Figs. 13 and 14) might be primarily due to one reaction. An attempt was therefore made to assign formation of the At^{211} and the Po^{210} in the peaks to a specific transfer mechanism. The three equations available from conservation of momentum and energy are (lab system)

$$P_b = P_R \cos\theta + P_X \cos\phi$$

$$P_R \sin\theta = P_X \sin\phi \qquad (10)$$

$$E_b = E_R + E_X + E^* - Q$$

The subscripts b, R and X denote bombarding particle, recoil product and projectile residue respectively. The angle between the beam direction and the recoil is θ, between the beam and the projectile residue, ϕ. Assumption of a mechanism defines the various masses and Q. Since the experimental measurements yield E_R and θ, Eqs. (10) may then be solved for E^*, E_X, and ϕ. Alternatively, an E^* appropriate to the proposed mechanism may be assumed and Eqs. (10) solved for θ. This predicted θ may then be compared with the experimentally observed θ_p; disagreement indicates a faulty choice of mechanism. The latter procedure has been carried out for a number of pertinent E^* values in Table VIII. As an example, consider Run XI. For At^{211} produced by 2p transfer, $0 \lesssim E^* \lesssim 7.6$. The θ predicted for such a reaction is then 57.7° to 55.0°. If At^{211} comes from an "(α,2n)" reaction, $10.9 \lesssim E^* \lesssim 18.5$ and the predicted θ is 48.0° to 45.6°. The experimental angular

distribution (Fig. 14) peaks at $\theta_p \approx 48°$ so that we might conclude that the At^{211} at this energy came from an α transfer reaction rather than a 2p transfer. In Run X also, the θ calculated for α transfer shows better agreement with experiment than the θ for 2p transfer. In this case, however, the C^{12} resulting has a greater velocity than it had when it was still part of the projectile (i.e. $E_{C^{12}} > 12/16\ E_b$); this may be unrealistic. Moreover, the experimental θ_p's for Po^{210} do not correspond well with the predicted θ's for any of the mechanisms tried. It would thus probably be wise to adopt a cautious attitude with regard to the (perhaps fortuitous) correlations in the At^{211} cases.

There are a large number of reactions which have not been considered in Table VIII. Among these are other multinucleon transfers and reactions where the projectile residue carries off excitation energy—perhaps sufficient for break-up (for example, $Bi^{209} + O^{16} \longrightarrow [At^{213}]^* + 3\alpha$). Consideration of these other reactions would be certainly very tedious and very difficult, and probably not very valuable as it is most unlikely that clear-cut decisions could be reached on the small amount of data presented here. It is better, then, to say that the calculations shown in Table VIII indicate (a) that At^{211} and Po^{210} at the higher bombarding energies probably do not come from simple p and 2p transfer reactions as observed near the barrier; (b) that α transfer may account for the production of At^{211}; and (c) that the data obtained here are incapable of providing enough detailed information to determine the reaction mechanisms unambiguously.

The Pb^{208} bombardments yielded results even more complex than the Bi runs. Fr and Rn are still produced, which indicates that transfer of at least 4 and 5 protons can occur. Some of the range distributions show definite evidence of multiple peaking (see Table III and Fig. 10). For some components, peaks may occur as deep in the stack as R_{TMT}. The angular distributions show strong forward peaking for Rn products, but At^{211} and Po^{210} again have large-angle contributions, particularly at 123 MeV (Figs. 15 and 16). Once again we must conclude

that a number of different transfer mechanisms, and possibly compound nucleus formation, are contributing to the products observed.

When all of the higher energy experiments on both Bi and Pb targets are considered, a fairly consistent picture of the qualitative features of transfer reactions emerges. Let us define a number, $\nu = Z_R - Z_\tau$ where R and τ denote recoil product and target respectively. This number, ν, is thus the net number of protons transferred into the target, and should bear some approximate relation to the gross number of nucleons transferred. The following remarks may then be made. (a) Except in those cases where contributions from TMT or near-TMT processes interfere, the rule generally holds that the higher the ν, the longer the projected recoil range. This is a quite reasonable result, as the amount of momentum transferred would be expected to roughly parallel the number of nucleons transferred. (b) If cross sections for the undetected products are estimated by interpolation and extrapolation among the measured products, and if appropriate adjustments for feed-in are made, both the Bi and Pb results indicate that the higher the ν, the lower the total cross section for that ν. For example, for Bi targets, $\sigma_{Po} > \sigma_{At} > \sigma_{Rn}$, where σ_{Po} denotes the total measured and estimated cross section for all Po isotopes, and so on. This implies that the probability for transfer falls off with increasing number of nucleons transferred. (c) For constant ν, the total cross sections from Bi and and Pb bombardments agree within the errors involved. For example, σ_{At} from the Bi bombardments agrees with σ_{Po} from the Pb runs. This implies that the transfer processes are not sensitive to small changes in the target. (d) The angular distributions also vary regularly with ν; these results are summarized in Table IX. For $\nu = 1$, which presumably corresponds to transfer of a very small number of nucleons, the heavy product peaks at a lab angle of around 50°. As ν increases the peak angle decreases steadily. That is, the heavier the projectile residue, the more the recoil is deflected from the beam direction.

The above results are in accord with a simple, semi-classical model for PMT reactions in which the number of nucleons transferred varies as the degree of overlap between the nuclear volumes of target and projectile. The results appear to differ from those of Kaufmann and Wolfgang.[5,37] They bombarded Rh^{103} targets with C^{12}, N^{14}, O^{16}, and F^{19} and studied the projectile residues C^{11}, N^{13}, O^{15} and F^{18} for each projectile. Although the products of single-nucleon transfer reactions showed peaking at wide angles, all multi-nucleon transfer products were peaked forward. In the present work, the peaking at large angles of the heavy fragments from multi-nucleon transfers implies that the lighter projectile residues must be even more widely peaked. Kumpf and Donets also report wide peaking of the heavy fragment from multi-nucleon transfers (they detected $Ac^{224,225,226}$ and Th^{227} from bombardments of Th^{232} with Ne^{22}).[52] It is possible that similar reactions do not occur for the lower mass target used by Kaufmann and Wolfgang.

The fact that, for $\nu = 1$ to 3, the residue peaks at wide angles means that breakup of such a residue can not produce the strongly-forward-peaked showers of α particles and protons seen by Britt and Quinton. The $\nu = 4$, 5 reactions may, however, contribute to this low angle production of small fragments.

* * *

Let us summarize this entire discussion in the following way. Many workers have used the measurement of the recoil ranges as a powerful tool for the study of nuclear reaction mechanisms, particularly when the mode of momentum transfer leading to the observed product is unique.[17-21] Recoil range methods can also be helpful when the momentum transfers of two mechanisms differ widely.[21,38] In this work, then, for the bombardments near the barrier we were able to derive specific

information regarding the reaction mechanisms. At the higher energies, where many mechanisms compete, the method is useful chiefly for survey purposes. Further work to investigate more fully the low energy region for Bi and Pb^{208} targets with different projectiles is certainly warranted.

(Late in the preparation of this report, a translation was obtained of a recent Russian paper which appears quite pertinent to this work. Lozhinski studies the angular distributions of the projectile residues from multi-nucleon transfer reactions of Ne^{20} ions with Cu, Rh, Ta, Au and U targets and Ar^{40} ions with Au.[39] The distributions show very slight large angle peaking for Cu, but as the mass of the target is increased, the peaking (a) becomes more and more pronounced and (b) appears at larger and larger angles. For the reaction of Au with Ar^{40} at 216 MeV, the Cl^{39} and S^{38} residues from p and 2p transfer had cross sections of 10 mb and 3 mb respectively—again a large relative probability for 2p transfer. These data are thus in excellent qualitative agreement with the results of the present work.)

IV. CONCLUSIONS

The major conclusions reached in this work are:

Al_2O_3 foils have been found satisfactory for use as catchers in range studies of heavy recoils, and in many ways these foils are easier to use than Al leaf. Ranges (in mg/cm^2) of At and Po nuclides of recoil energy 6 to 12 MeV are 7 to 11% greater in Al_2O_3 than in Al leaf; range straggling in Al_2O_3 is about 20% less in Al_2O_3 than in Al leaf.

For O^{16} bombardments of Bi^{209} at energies near the barrier, production of Po^{210} and At^{211} occurs by p and 2p transfer mechanisms, with the projectile remnant being ejected in a backward direction. For O^{16} energies greater than about 1.3 times the Coulomb barrier, many transfer reactions contribute to production of various Po, At, Rn, and Fr nuclides from both Bi and Pb^{208} targets. Alpha transfer may be a possible reaction, but no evidence was obtained to suggest that this might be a preferred mode. Full momentum transfer reactions contribute very little to the production of the above products from the Bi targets, but may produce some of the Fr and Rn from Pb^{208}.

ACKNOWLEDGMENTS

I wish to thank my research director, Professor Kenneth Street, Jr., for his continued help and guidance throughout the course of this work.

I am grateful to Victor E. Viola, Jr., who suggested this research and whose assistance in its early stages inestimably reduced the length of the "fumbling" period.

Sincere thanks are due Professor John M. Alexander for many helpful suggestions; without his interest and encouragement, this work would not have been possible.

Conversations with Jacob Gilat and Lawrence L. Altman were frequently pertinent to the research, and were greatly appreciated. Conversations with M. L. Hyder, R. L. Kiefer, R. G. Korteling, J. D. Mahony, J. B. Nash, J. A. Olmsted, III, A. J. Pape, C. F. Smith, Jr., and B. D. Wilkins were perhaps less often pertinent, but were equally appreciated. The contributions of Charles Goren and Alvin Dark to these conversations cannot possibly be ignored.

I am indebted to Duane F. Mosier for essential lessons in the care and feeding of the temperamental grid chamber and its associated electronics. I thank the Hilac operating crew, particularly the owl shift, for efforts often well beyond the call of duty.

This work was performed under the auspices of the U. S. Atomic Energy Commission.

Table I. Recoil studies of At , Po in Al and Al_2O_3

Stopper	Projectile	Beam Energy E_b (MeV)	Total Degrader (mg/cm^2 Al)	Target Thickness (μg/cm^2)	R_m (μg/cm^2)	ρ	E_{TMT} (MeV)	Probable A_R	Reference	E/amu
Al	O^{18}	72.4	42.1	64	410	0.23	6.06	207	17	.02927
		112.9	30.3	64	598	0.19	9.27	203		.04566
		130.9	23.9	75	670	0.20	10.69	202[a]		.05292
					635	0.29	10.80	204		.05294
		148.1	17.2	72	732	0.26	12.10	202		.05990
		164.5	10.3	78	770	0.24	13.37	201		.06651
		182.9	2.0	75	807	0.23	14.75	199.5		.07893
	O^{16}	81.3	32.7	44	419	0.28	6.10	205	This work	.02975
		102.9	25.9	38	522	0.25	7.61	201		.03786
		128.3	16.6	47	626	0.25	9.45	200.5		.04713
		140.0	11.7	44	651	0.24	10.23	200		.05115
		152.3	6.2	39	679	0.25	11.10	199		.05577
		162.9	1.6	38	680	0.25	11.84	198.5		.05964
Al_2O_3	O^{16}	80.3	32.9	39	445	0.19	6.06	204[+]	This work	.02970
		91.5	29.0	44	500	0.19	6.89	203.5		.03385
		109.3	23.7	44	584	0.18	8.24	203[-]		.04059
		123.4	18.4	39	647	0.20	9.18	201[+]		.04567
		147.8	8.4	39	725	0.21	10.88	199		.05467
		162.6	1.6	44	782	0.22	11.94	198.5		.06015

[a]Two components separated. See Table III, Reference 17.

Table II. Half lives and α energies of observed products.

This work		Assignment	Previous work		
α Energy (MeV)	$t_{1/2}$		α Energy (MeV)	$t_{1/2}$	Reference
6.40	15-30 min	Fr^{212}	6.42, 6.39	19.3 min	43
6.26	25.5 min	Rn^{212}	6.26_4	23 min	43
6.04	2.42 hrs	Rn^{210}	6.03_7	2.7 hrs	44
5.65	5-6 hrs	At^{209}	5.65	5.5 hrs	29
5.30	135-140 days	Po^{210}	5.29_8	138.4 days	29
5.11	2-4 yrs	Po^{208}	5.10_8	2.9_3 yrs	29
5.22	~ 9 days	Po^{206}	5.21_8	8.8 days	29
~5.86 and 7.44	14.6 hrs and 7.25 hrs	Rn^{211}-At^{211}-Po^{211} chain	5.85, 5.78 5.86, 7.44 et al.	16 hrs 7.214 hrs 0.52 sec	44 47 29

Underlined half lives are those used in decay analysis.

Table III. Range distributions.

Run No.	Target Nuclide	Target Thickness ($\mu g/cm^2$)	E_b (MeV)	E_b (c.m.) / E_{Coul}	Product[a]	Activity in: Tgt.	1	2	3	4	5	6	7	8	9	10	11	12	13	14	15	Range (No. Al_2O_3 foils) R_p[b]	R_m	R_a	R_{TMT} (At^{211})	Approx. σ (mb)
I	Bi	143	$162._3$	2.00	Rn^{212}	70	1180	2550	3580	1415	980	620	340	230	170	120						2.7	3.06	3.45		21
					Rn^{211}	70.2	157.4	291.0	236.6	110.7	44.9	12.8	7.0									2.2	2.32	2.48		14
					Rn^{210}	273	690	1285	1015	475	275	160	90	60	45	31						2.4	2.51	2.87		14
					At^{211}	434	652	846	508	181	68	21	11									2.0	1.81	1.97	10.5	30
					At^{209}	67	69.5	81	64	32	~19	~10	~5.5	~4								2.3	1.86	2.04		39
					Po^{210}	8.4	9.9	11.0	5.8	1.9	~1											2.0	1.62	1.73		97
					Po^{208}	.85	1.04	.82	.28	.13	.06	~.01										1.4	1.27	1.50		63
II	Bi	41	$162._3$	2.00	Fr^{212}		~30	~79	159	141	120	60	~40	~30	~21	(←	~30	→)				3.2	3.70	4.35		3
					Rn^{212}	34	221	1100	1720	1115	640	314	170	105	64	49	43	~30				2.7	3.02	3.42		11
					Rn^{211}	5.0	53.5	277.8	260.0	136.4	60.3	29.1	14.5	10.3	6.4	4.1	3.6					2.1	2.50	2.84		12
					Rn^{210}	18.5	196	930	1120	515	204	$112._5$	$66._5$	55	47	32	28	20				2.3	2.59	3.07		11
					At^{211}	49.3	352.9	908.2	713.6	214.2	51.4	17.4	6.8	1.7	1.0							2.0	2.01	2.09	10.5	24
					At^{209}	7.3	53.4	86.5	59.8	29.5	11.6	3.2	2.5									1.8	1.91	2.12		27
					Po^{210}	1.12	7.41	11.78	6.63	1.91	.51	.21	.07									1.9	1.68	1.80		76
					Po^{208}	.14	.80	1.06	.76	.15	.04	.03	$.00_4$									1.6	1.59	1.76		59
III	Bi	71	$152._3$	1.88	Fr^{212}		<7.3	$60._5$	116	63	31	25	(~20)		8							2.8	3.15	3.56		2
					Rn^{212}	15	161	726	921	700	430	231	114	87	43	42						2.7	3.15	3.52		10
					Rn^{211}	3.4	31.3	112.4	100.7	49.7	24.9	12.0	6.4									2.2	2.46	2.70		8
					Rn^{210}	15	98	313	366	188	94	$55._5$	25	19	23	9						2.4	2.70	3.1		6
					At^{211}	32.8	204.9	393.2	279.8	117.0	42.7	12.1	<4.5									2.1	2.06	2.19	10.0	18
					At^{209}	4.8	26.4	40.8	26.8	12.8	4.8	2.4	1.3	1.0	0.7	0.5						1.8	1.98	2.27		20
					Po^{210}	1.01	2.73	4.66	3.01	1.08	.40	.16	.11	.08	.06	.04						1.9_5	1.89	2.10		54
					Po^{208}	.16	.29	.34	.22	.05	$.01_5$											1.8	1.65	1.68		32
IV	Bi	44	$123._2$	1.52	Fr^{212}			~8	12	15	20	12	28	16	18	13	5	3				6.4	6.07	6.91		1
					Rn^{212}	<12	109	470	498	520	310	260	190	170	94	74	78	35				2.7	3.67	4.33		12
					Rn^{211}	2.2	6.6	42.6	52.7	42.8	25.4	14.6	10.5	6.9	4.8	3.2	2.1	1.0				2.7	3.15	3.68		7
					Rn^{210}	1	7.2	34.9	38.3	31.6	22.1	15.6	9.9	9.4	6.6	3.9	3.4	3				2.5	3.44	4.11		1
					At^{211}	20.5	135.1	335.5	498.1	375.8	201.9	125.4	60.7	27.2	14.2	7.0	3.0	1				2.9	2.93	3.20	8.3	43
					At^{209}	1.6	13.8	25.8	27.8	18.4	14.8	7.8	3.7	2.6	2.4	<1.5						2.4	2.79	3.17		3
					Po^{210}	.27	1.29	3.46	4.34	3.31	1.76	.91	.43	.22	.10							2.6	2.80	3.01		95
					Po^{208}	.04	.11	.20	.22	.17	.10	.05	$.04_5$	$.03_5$	.02							2.4	2.54	2.80		33
V	Bi	118	$110._2$	1.36	Rn^{212}	30	35	160	300	340	330	241	160	112	50							3.9	4.45	4.78		3
					At^{211}	57	165	362	527	579	481	318	188	101	~50	~24						3.5	4.01	4.06	7.5	18
					At^{209}	3.4	8.5	15.2	15.1	15.0	16.3	9.2	8.4	5.6	3							3.3	3.89	4.08		6
					Po^{210}	.56	1.12	2.35	4.01	4.56	4.30	2.73	1.50	.70	.34							3.8	4.08	4.16		32
					Po^{208}	.02	.05	.09	.13	.15	.12	.10	.06	.03	.01							3.8	3.88	3.92		6
VI[c]	Bi	84	$85._2$	1.05	At^{211}																	~9.5			6.2	12
					Po^{210}																	>10				19
VII[d]						Foil[d]	9	10	11	12	13	14	15	16	17	18	19	20								
	Bi	73	$75._8$	0.93	At^{211}		12.1	17.0	30.0	50.0	62.0	84.6	77.6	75.6	51.6	29.2	9.8	~5				14.3	14.38	14.19	5.4	5
					Po^{210}		.10	.15	.21	.32	.40	.58	.67	.67	.62	.50	.33	.2				15.8	15.88	15.3		11

Table III. (Continued)

Run No.	Target: Nuclide	Target: Thickness ($\mu g/cm^2$)	E_b (MeV)	E_b (c.m.) / E_{Coul}	Product[a]	Activity in: Tgt.	1	2	3	4	5	6	7	8	9	10	11	12	13	14	15	Range (No. Al_2O_3 foils): R_p[b]	R_m	R_a	R_{TMT} (At^{211})	Approx. σ (mb)
VIII	Pb^{208}	44	$162._3$	2.02	Fr^{212}		<1	<2	~16	21	50	32	<23	40	56	31	37	25	15			~4.7, ~8.5, (10.7)	7.9	7.6		~2
					Rn^{212}		60	314	661	703	500	345	310	310	370	205	190	125	70			3.4, (~8.7)	4.83	5.58		12
					Rn^{211}	3.2	13.2	60.4	148.7	159.0	105.3	53.4	30.2	20.0	14.8	14.9	12.5	8.2				3.3, (9.7)	3.66	4.32		13
					Rn^{210}	10.8	41.5	218	590	638	475	287	179	149	109	80	61.5	41	25			3.3	4.06	4.72		15
					At^{211}	6.2	42.5	137.6	112.1	590	26.3	15.6	7.5	5.1	2.4							2.0	2.31	2.64	10.5	7
					At^{209}		6.9	22.2	25.1	20.7	11.8	7.4	8.2	3.7	4.5	<3	2	1.3	1.0			2.7, (6.7?)	3.35	4.08		20
					Po^{210}	.37	1.98	3.63	2.43	1.02	.40	.20	.12	.06	.04							1.7	1.90	2.17		44
					Po^{208}	.09	.47	.66	.43	.24	.10	.06	.04	.03	.03							1.4	1.84	2.13		57
					Po^{206}	.20	.98	1.94	1.18	.83	.50	.30	.20	.16	.11							1.4	1.69	1.92		23
IX	Pb^{208}	41	$123._2$	1.53	Rn^{212}	2.5	12	110	219	200	220	195	90	42.5	31.5	24.8	10.5	6.3	3.2	1.0	.6	3.8	4.34	4.54		9
					Rn^{211}	.3	3.0	14.4	34.4	42.9	66.5	86.6	76.7	51.8	37.7	25.2	16.8	10.8	5.6	3.0	1.8	5.9, (~33)	6.04	6.22		12
					Rn^{210}	.6	1.4	4.8	8.3	20.0	31.0	70.0	81.0	78.5	73.0	64.1	52.0	34.0	18.5	8.1	5	~6.8	7.93	8.03		5
					At^{211}	3.4	21.8	79.9	88.0	57.8	37.8	28.2	21.2	13.6	10.0	6.2	3.0	1.1	1.4			2.3	3.11	3.68	8.4	8
					At^{209}	all max. values (1.0	.8	1.3	2.0	.8	2.8	3.3	2.5	1.6	.8	.4	.3	.1)				~7.6	~7.1	~6.8		<4
					Po^{210}	.32	.80	2.11	2.29	1.61	.98	.58	.35	.27	.20	.22	.15	.10				2.3	2.92	3.50		43
					Po^{208}		.13	.29	.22	.20	.14	.07	.05	.08	.03	.02						2.0, (7.6)	2.6	3.26		31
					Po^{206}																					<4

[a] "Po^{210}" data includes (Bi^{210} + Po^{210} + At^{210}).

"Po^{208}" data includes (Po^{208} + At^{208}).

[b] Parentheses indicate lesser peaks.

[c] Accidental foil breakage precluded full distribution measurement.

[d] Note change in foil numbering—Run VII only.

Table IV. Angular Distributions

Run No.	Target	E_b (MeV)	Product	[a]Range / [b]Activity at median angle listed: 13.0	21.8	30.7	39.6	48.3	57.0	65.8	74.4	83.0	θ_p deg.	R_{θ_p} ($\mu g/cm^2$)	Recoil Energy E_R (MeV)	$\bar{R}_{proj}$ (Al_2O_3)	R_m^c foils
X	Bi^{209}	$161._6$	Rn^{211}	[a] 182	180	185	182	142	90							2.2_2	2.4_1^d
				[b] 46.1	36.9	39.2	31.0	10.1	3.6								
			Rn^{210}	180	182	175	187	(142)	(90)							2.2_2	2.5_5^d
				117.7	72.4	74.6	62.2	(20.2)	(7.2)								
			At^{211}	260	~100	116	121	194	172	127	108		~48	174	2.4_7	1.6_9	1.9_1^d
				12.4	7.4	6.1	24.5	75.9	27.0	~5	~1.5						
								(55.7)	(20.8)								
			Po^{210}	131	147	131	100	199	179	204	100		~55	194	2.7_5	1.7_1	1.6_5^d
				.108	.111	.111	.220	.331	.234	.263	.014						
XI	Bi^{209}	$122._2$	Rn^{211}	275	229	246	321	280	352							3.2_5	3.1_5
				46.8	48.2	67.5	60.6	55.5	10.8								
			Rn^{210}	308	238	210	(321)	(280)	(352)							3.2_2	3.4_4
				63.7	62.5	81.1	(77.9)	(71.3)	(13.9)								
			At^{211}	132	171	134	325	310	300	248	241		~48	311	4.4_8	2.9_1	2.9_3
				25.3	24.6	37.8	228.3	265.5	156.6	21.6	11.5						
							(150.4)	(194.2)	(132.7)								
			Po^{210}	226	203	190	278	326	310	326	274	~230	~51	308	4.4_0	2.7_7	2.8_0
				.291	.278	.312	.575	.742	.718	.224	.068	<.020					
XII	Pb^{208}	$161._6$	Rn^{211}	265	284	262	314									3.8_2	3.6_6
				117.1	73.4	28.0	~5										
			Rn^{210}	311	319	290	(314)									4.3_4	4.0_6
				215.6	117.4	48.0	(~8.6)										
			At^{211}	281	130	189	224	211	~112	~100						2.3_3	2.3_1
				12.8	14.1	11.2	22.3	7.6	2.1	~1.5							
							(13.7)										
			Po^{210}	316	210	194	185	159	155	~174						2.1_8	1.9_0
				.188	.159	.171	.154	.212	.078	.031							
XIII	Pb^{208}	$122._2$	Rn^{211}	561	359	~272										7.1_9	6.0_4
				103.6	22.2	2.8											
			Rn^{210}	639	342	(~272)										7.8_7	7.9_3
				87.9	21.7	(2.7)											
			At^{211}	255	291	304	279	280	~211				~34	291	4.1_9	3.5_0	3.1_1
				2.6	4.1	25.1	18.3	4.4	<0.9								
						(22.4)											
			Po^{210}	202	129	222	311	282	211	239	241		~46	270	3.0_0	2.8_5	2.9_2
				.061	.053	.058	.133	.195	.071	.024	.018						

[a]Upper figure is range, R_θ in $\mu g/cm^2$ Al.

[b]Lower figure is activity (arbitrary units) of entire foil stack at θ.

[c]R_m values taken from Table III at corresponding E_b.

[d]Average of two runs.

(Parentheses indicate estimated values—see text.)

Table V.

E_R (MeV)	Ranges (mg/cm^2) in stopper indicated					Range Ratio Al_2O_3/Al
	N_2[a]	Ne[a]	O_2(interpolated)	Al[b]	Al_2O_3(Eq. 5)	
14.1	0.973	1.272	1.073	0.970	1.015	1.05
5.8	0.465	0.571	0.500	0.449	0.472	1.05

[a]Reference 32.

[b]References 17, 18.

Table VI. Reaction Q values.

Reaction					Q (MeV)
$Bi^{209} + O^{16}$	$\longrightarrow$	At^{213}	+	C^{12}	-16.6
	$\longrightarrow$	At^{211}	+	C^{14}	-14.4
	$\longrightarrow$	Po^{211}	+	N^{14}	-13.4
	$\longrightarrow$	Po^{210}	+	N^{15}	- 7.2
	$\longrightarrow$	Bi^{210}	+	O^{15}	-10.1
$Pb^{208} + O^{16}$	$\longrightarrow$	Po^{212}	+	C^{12}	-16.2
	$\longrightarrow$	Po^{210}	+	C^{14}	-13.6
At^{213}	$\longrightarrow$	At^{211}	+	2 n	-10.9
At^{213}	$\longrightarrow$	Po^{210}	+	2 n + p	-13.9
At^{211}	$\longrightarrow$	At^{210}	+	n	- 7.6
Po^{212}	$\longrightarrow$	Po^{210}	+	2 n	-10.6
Po^{211}	$\longrightarrow$	Po^{210}	+	n	- 4.6
Po^{210}	$\longrightarrow$	Po^{209}	+	n	- 7.7
Bi^{210}	$\longrightarrow$	Bi^{209}	+	n	- 6.9

Table VII. Mechanisms for production of Po^{210} from O^{16} + Bi

Transfer of	to Yield	Followed by	to Yield	Followed by	to Yield	E^{*a} Requirement (MeV)	Calculated E^* (MeV)
2p	$[At^{211}]^*$	-n	At^{210}	ϵ	Po^{210}	$\gtrsim 7.6$	- 7.9
pn	$[Po^{211}]^*$	-n	Po^{210}			$\gtrsim 4.6$	- 6.9
p	$[Po^{210}]^*$					$\lesssim 7.7$	3.9
n	$[Bi^{210}]^*$			β^-	Po^{210}	$\lesssim 6.9$	1.0

[a]The E^* values are the appropriate neutron binding energies from Table VI.

Table VIII. Comparison of experimental angular peaking with predicted peaking for certain reactions.

Run	E_b (MeV)	Product	E_R (MeV)	θ_p(expt.) deg.	"Reaction"	E^{*a} (MeV)	θ(calc.) deg.	E_x (MeV)	$\left(\frac{m_x}{16}\right)E_b$ (MeV)
X	$161._6$	At^{211}	2.4_7	~48	2p	0	62.2	144.7	141.4
						7.6	59.3	137.1	
					α, 2n	10.9	49.0	131.6	121.2
						18.5	46.0	124.0	
		Po^{210}	2.7_5	~55	p	0	68.6	151.6	151.5
						7.7	65.7	143.9	
					α, 3n	18.5	46.8	123.7	121.2
						26.2	44.3	116.0	
					α, p2n	13.9	48.5	128.3	121.2
						21.6	45.6	120.6	
XI	$122._2$	At^{211}	4.4_8	~48	2p	0	57.7	103.3	106.9
						7.6	55.5	95.7	
					α, 2n	10.9	48.0	90.2	91.6
						18.5	45.6	82.6	
		Po^{210}	4.4_0	~51	p	0	63.0	110.6	114.6
						7.7	60.2	102.9	
					α, 3n	18.5	45.5	82.6	91.6
						26.2	42.6	74.9	
					α, p2n	13.9	47.0	87.2	91.6
						21.6	44.3	79.5	

[a]The E* values are appropriate neutron binding energies from Table VI.

Table IX. Summary of angular distribution results.

$\nu = Z_R - Z_\tau$	Example	Angular Distribution
1	Po from Bi	Pronounced peaking at lab angles $\gtrsim 50°$
2	At from Bi Po from Pb	Pronounced peaking at lab angles ~40° to ~50°
3	Rn from Bi At from Pb	Evidence of peaking at lab angles ~30° to ~40°
4	Fr from Bi Rn from Pb	Peaked strongly forward
5	Fr from Pb	Peaked strongly forward

Table X. Maximum possible cross sections for unobserved particles.

Product	Rn^{209}	Rn^{208}	At^{210}	At^{208}	At^{207}	Po^{209}	Po^{207}	Bi^{210}
Max. cross section	$1/2\ \sigma_{Rn^{210}}$	$1/4\ \sigma_{Rn^{212}}$	$\sigma_{Po^{210}}$	$\sigma_{Po^{208}}$	~ 6 mb	~ 6 b	~ 2 b	~ $\sigma_{Po^{210}}$

Table XI. Effect of errors on energy-momentum calculations. See Appendix C for discussion.

Line	Possible Product	Particle(s) Transferred	E_b (MeV)	E_R (MeV)	θ deg.	E* (MeV)	Remarks
1	At^{211}	α	75.8	15.8	0	-3.8	Impossible
2		2p				8.1	E* may be high
3	Po^{210}	p		17.9		3.9	Acceptable
4	At^{211}	α	78.5	15.8	0	1.3	α transfer possible, but not $\rightarrow At^{211}$
5		2p				9.0	At^{211} formed probably loses neutron
6	Po^{210}	p		17.9		8.8	Po^{210} formed probably loses neutron
7	At^{211}	2p	75.8	15.9	5	6.2	Acceptable
8				16.2	10	0.9	Acceptable
9	At^{211}	α	83.7	15.8	0	10.9	At^{211} from α transfer just possible
10	At^{211}	2p	75.8	16.6	0	2.4	Acceptable
11				18.9		-10.4	Impossible
12	Po^{210}	p	75.8	18.5	0	0	Maximum $E_{Po^{210}}$ possible

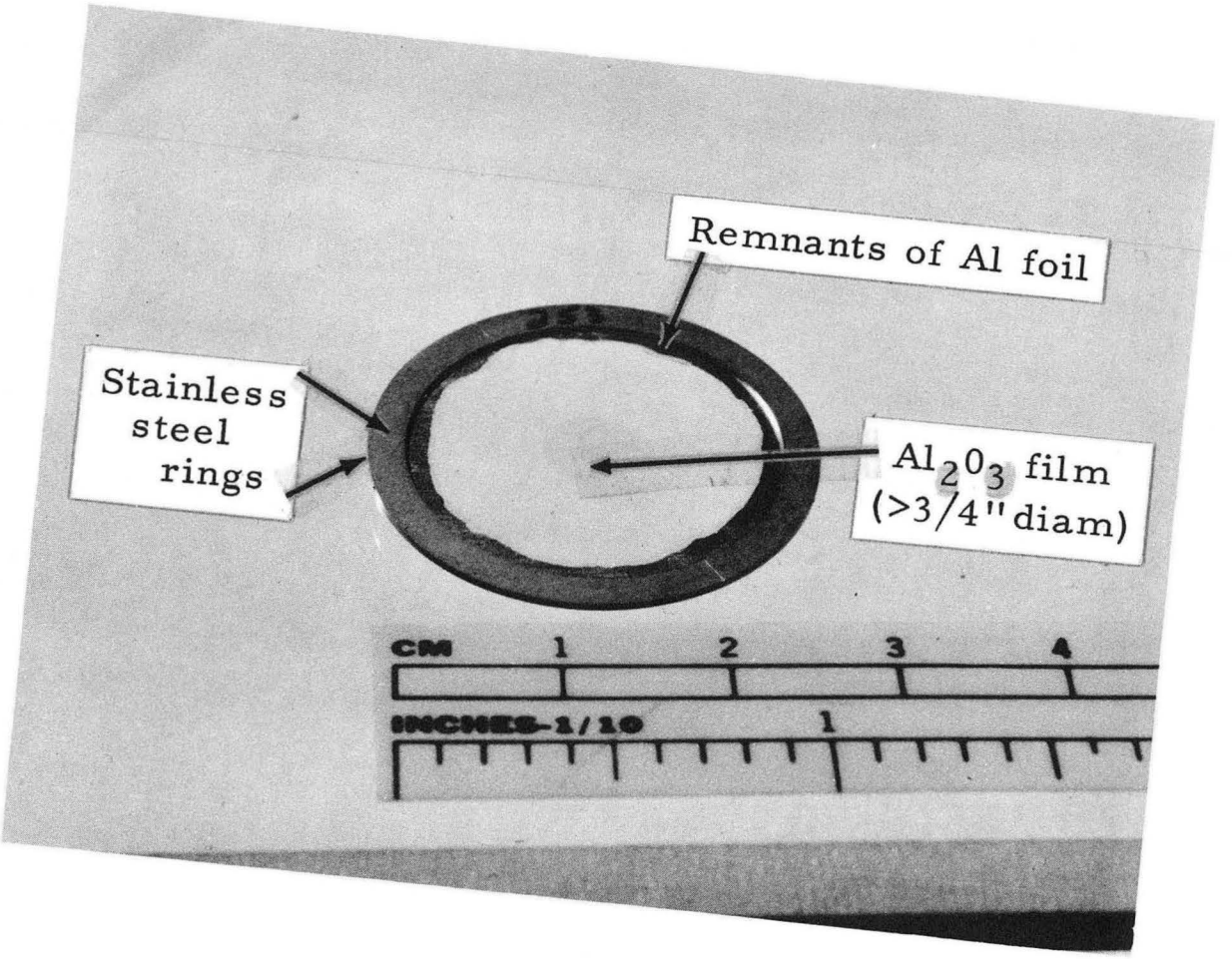

Fig. 1. Mounting of Al_2O_3 foils. Details of assembly are described in the text. Note "beam spot" at center.

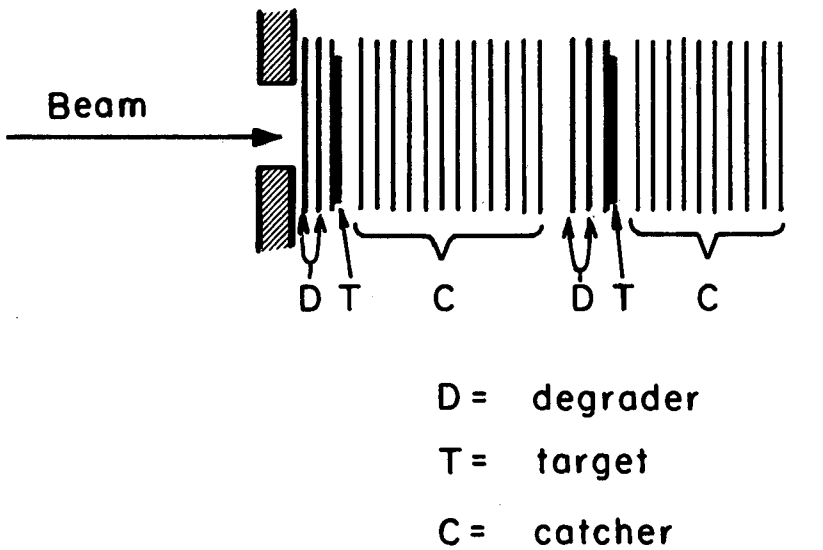

Fig. 2. Schematic of Al leaf foil stacking.

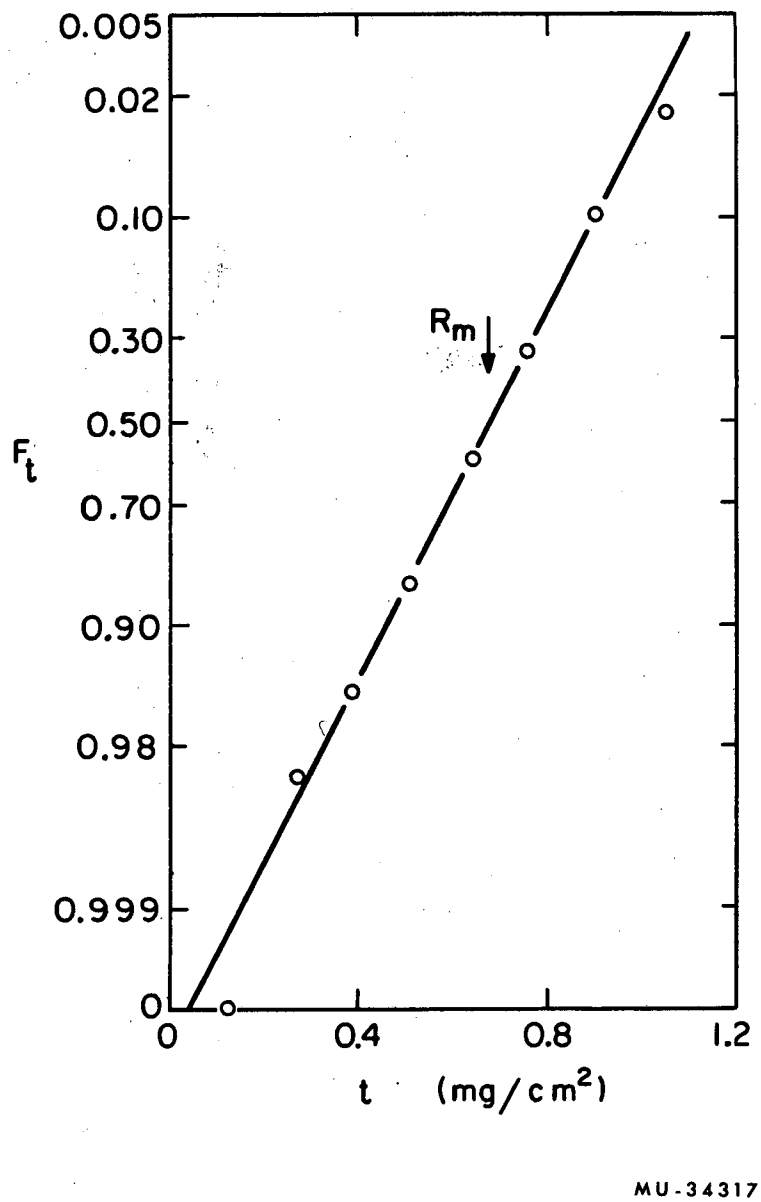

Fig. 3. A typical probability plot for an Al leaf experiment. The fraction F_t of the total activity that passed through catcher foils of combined thickness t is plotted against t.

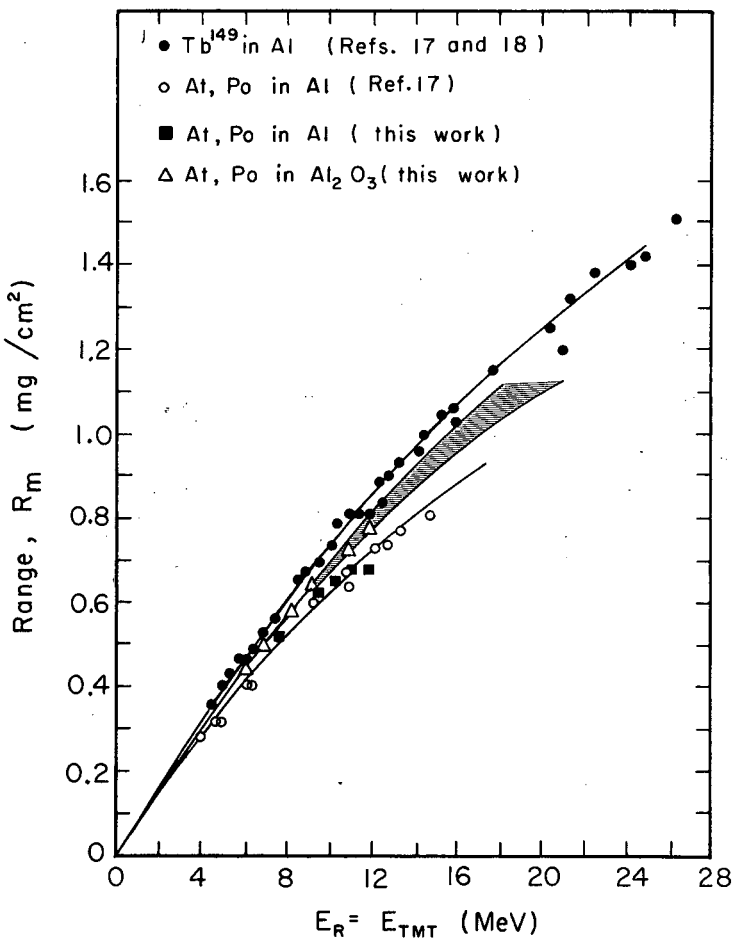

Fig. 4. Range-energy data. The shaded area indicates possible difficulties in extrapolating the Al_2O_3 curve.

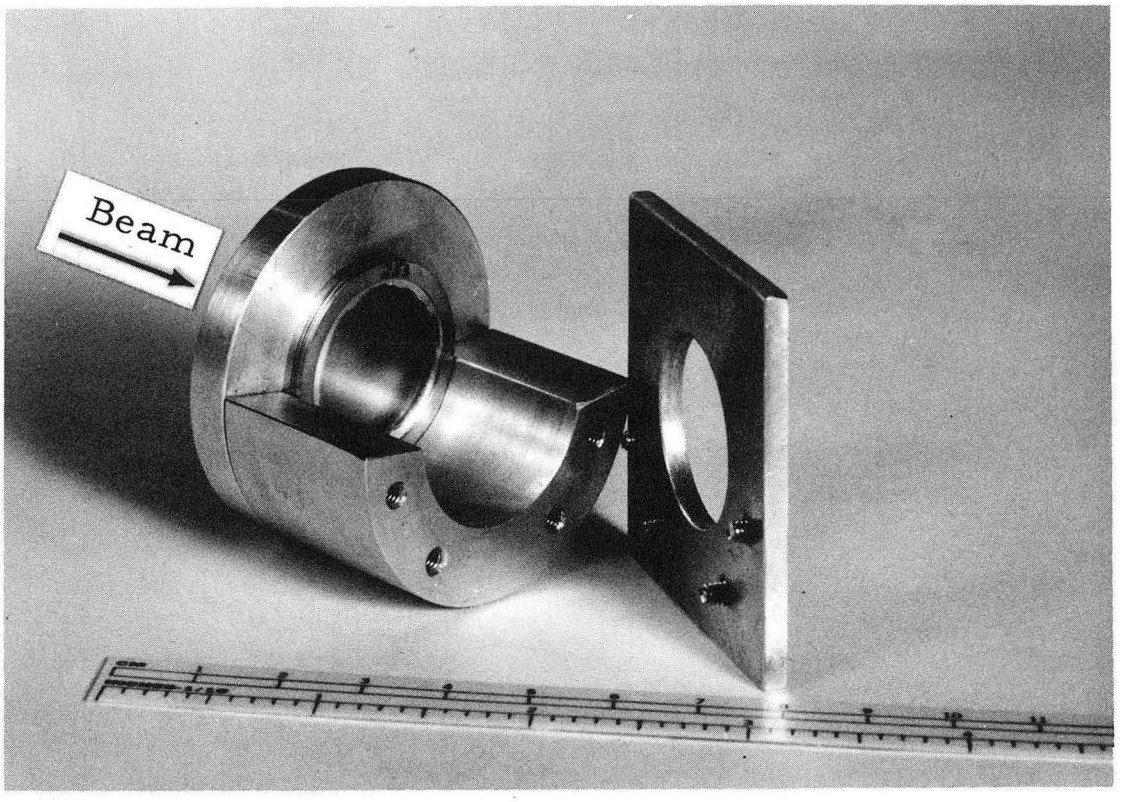

ZN-4353

Fig. 5. Foil holder for Al_2O_3 experiments. The target and first few catcher foils are in place.

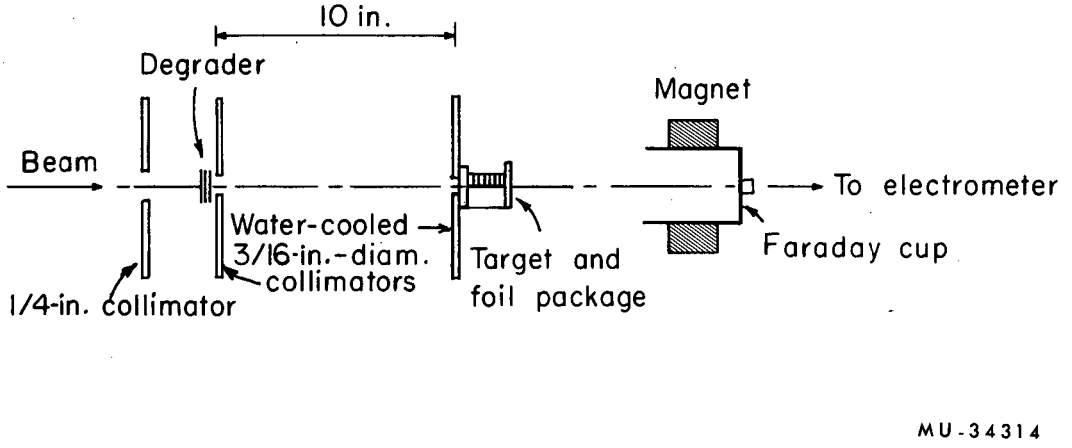

Fig. 6. Schematic of bombardment arrangement for Al_2O_3 runs.

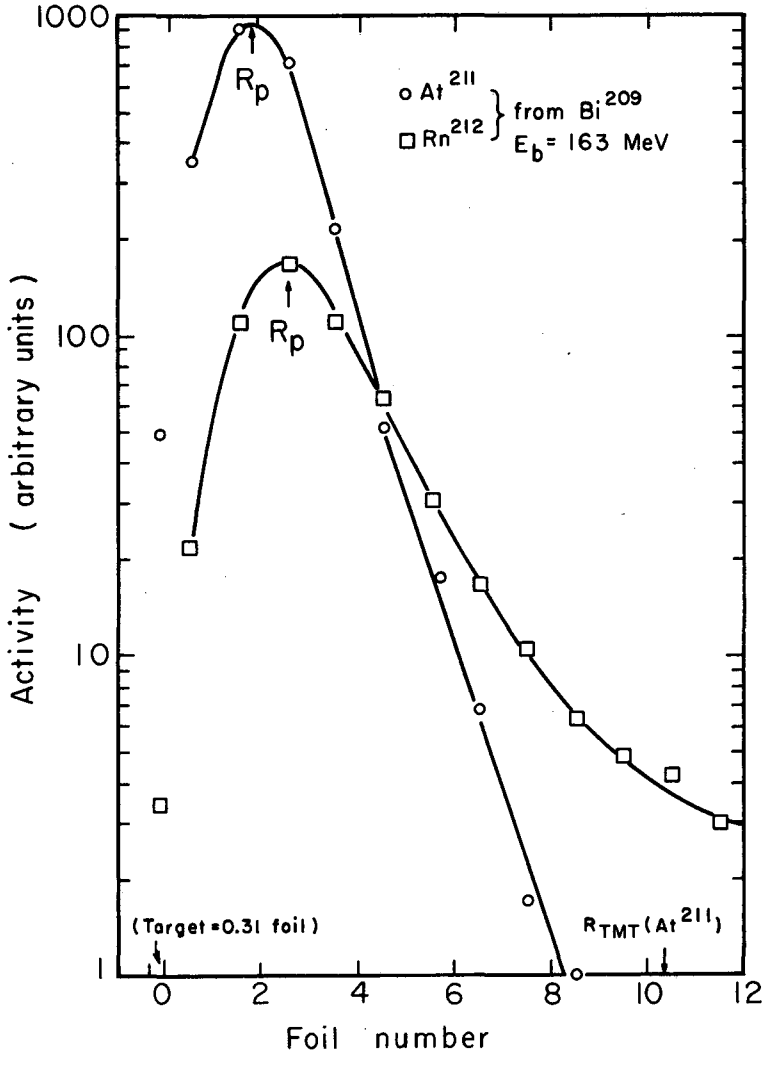

MU-34318

Fig. 7. Range distributions. The activity found in each foil is plotted against foil number. Each foil is 70.2 $\mu g/cm^2$ thick.

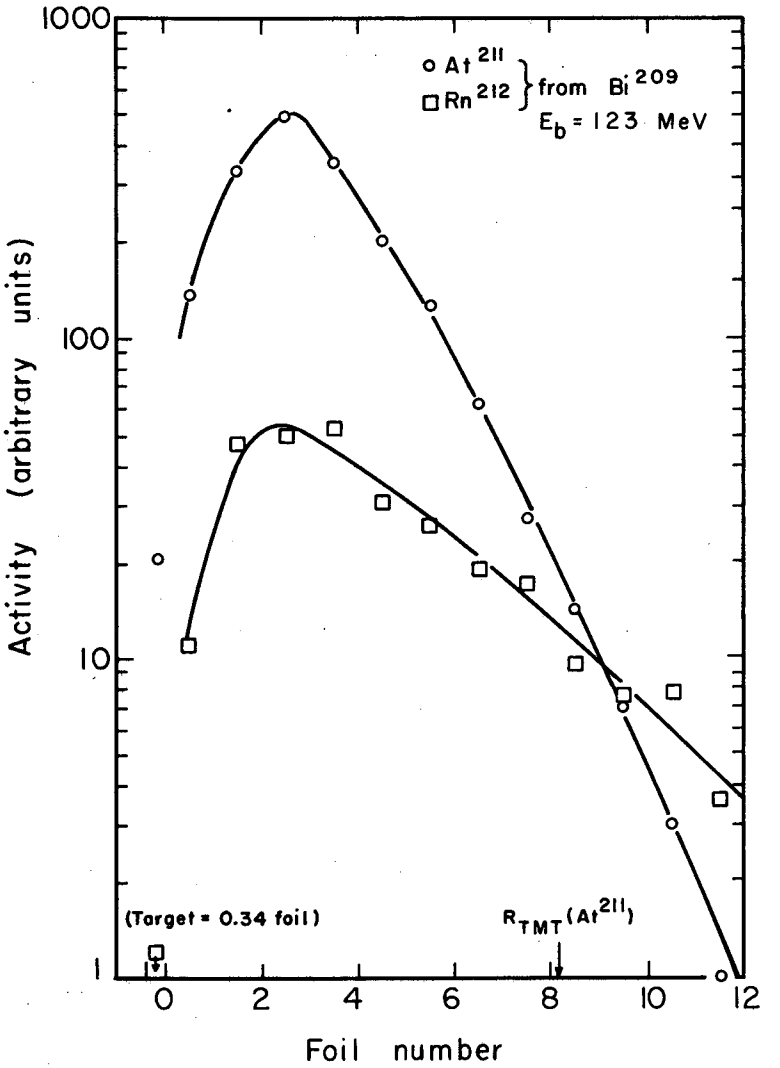

Fig. 8. Range distributions. The activity found in each foil is plotted against foil number. Each foil is 70.2 μg/cm^2 thick.

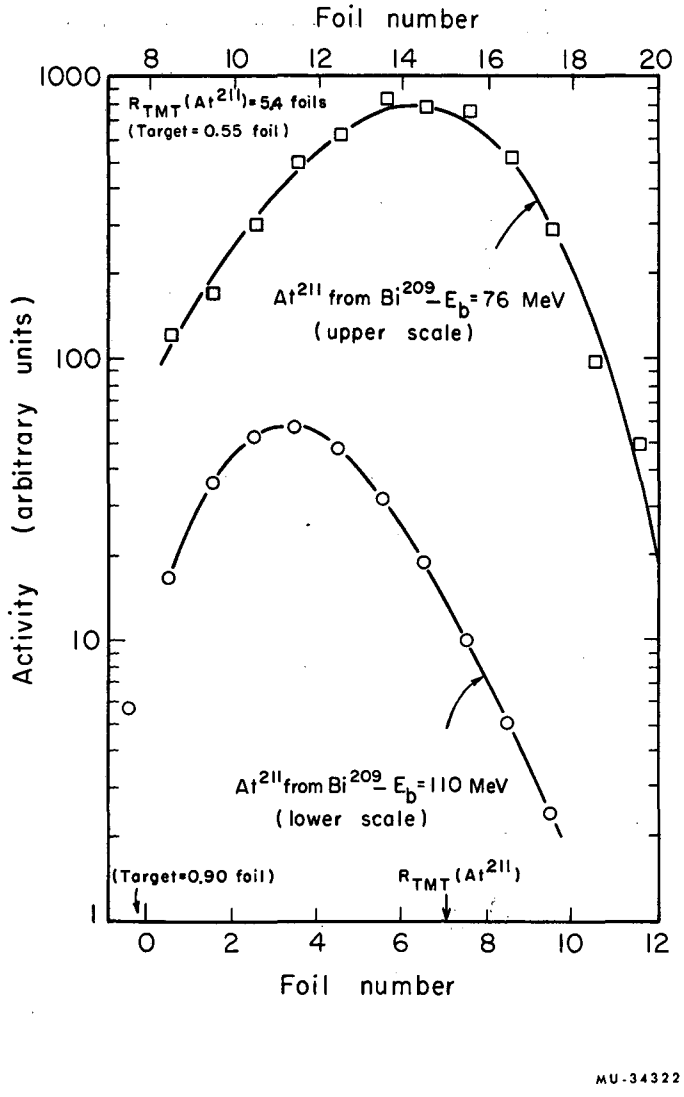

Fig. 9. Range distributions. The activity found in each foil is plotted against foil number. Each foil is 70.2 μg/cm^2 thick. Note difference in horizontal scales.

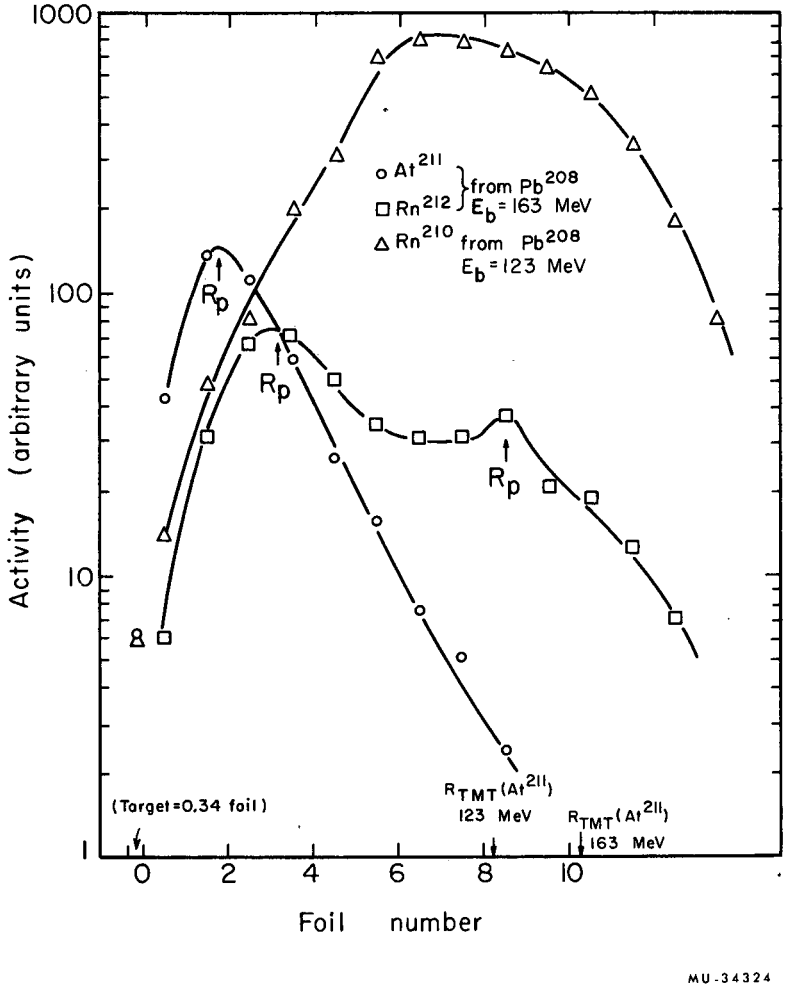

Fig. 10. Range distributions. The activity found in each foil is plotted against foil number. Each foil is 70.2 $\mu g/cm^2$ thick.

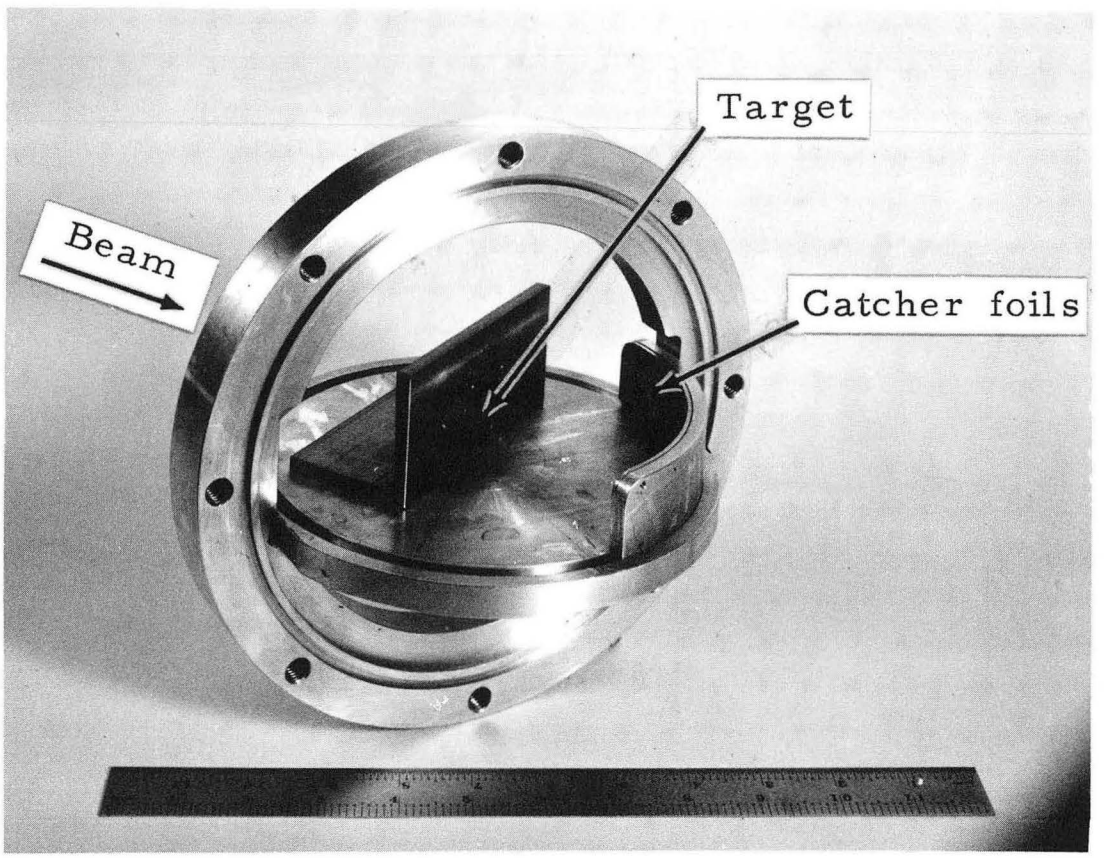

ZN-4352

Fig. 11. Angular distribution apparatus.

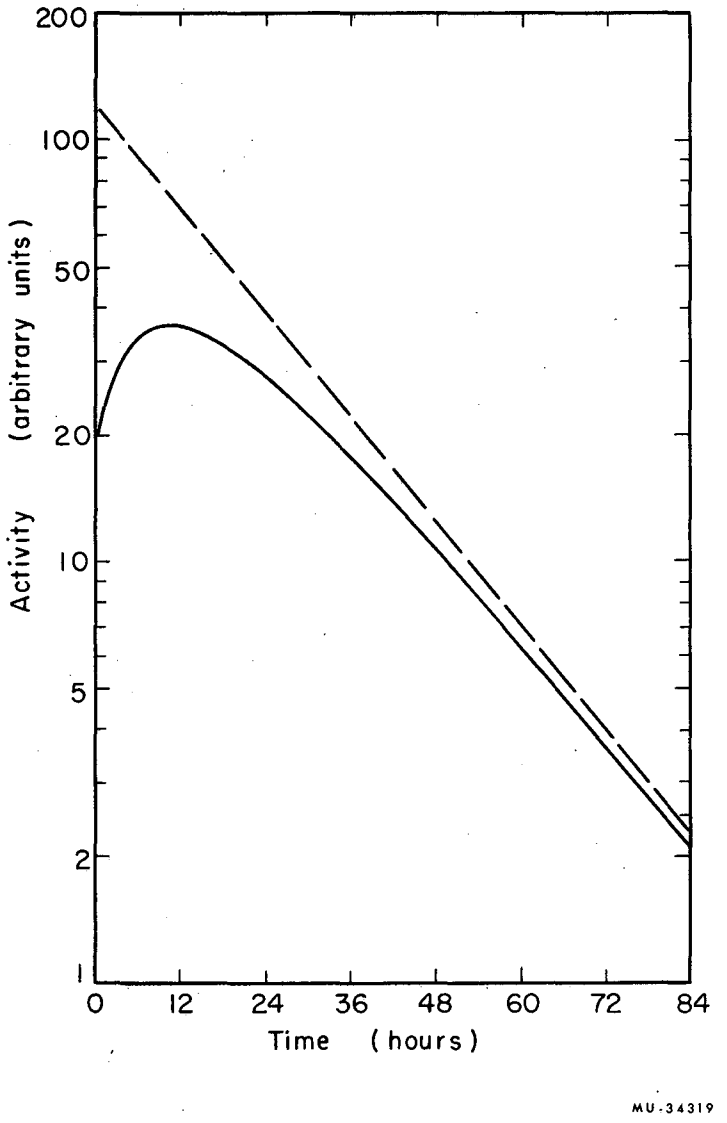

Fig. 12. The gross α activity from pure Rn^{211} plotted against time. The dashed line is the asymptote.

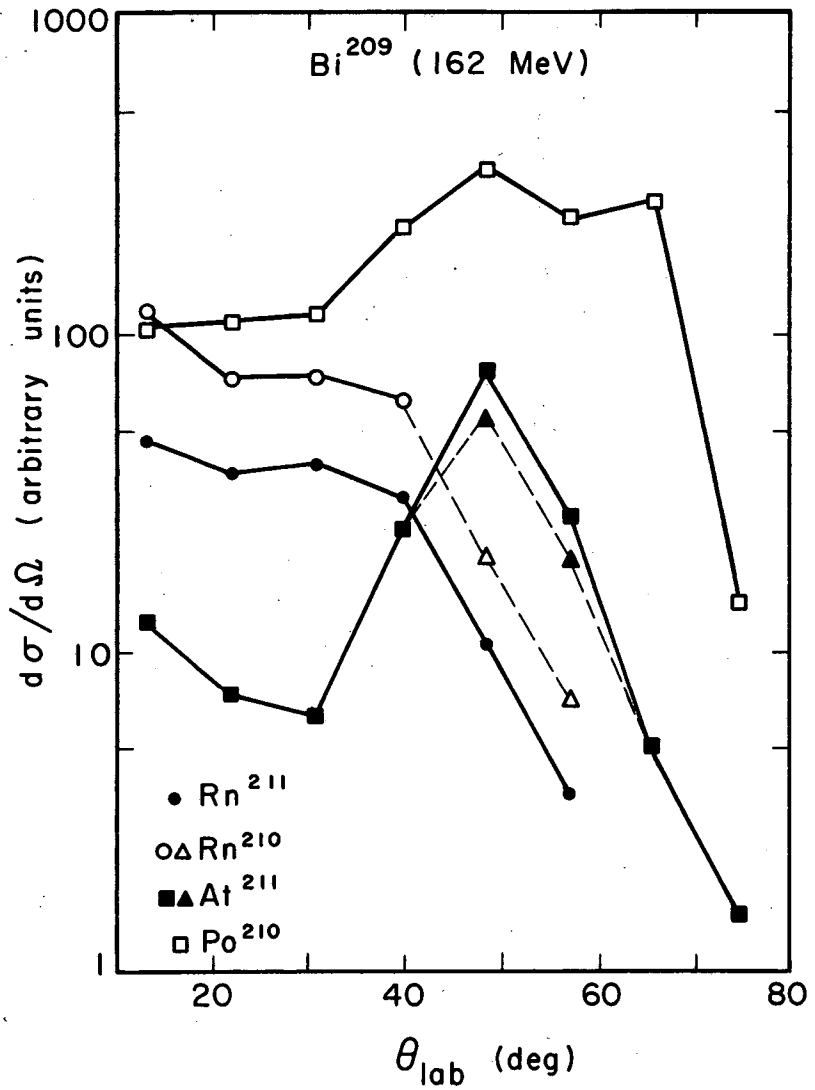

Fig. 13. Angular distributions. The differential cross section (arbitrary units) is plotted against the median angle of each collection segment. The circles, squares and solid lines are experimental data. The triangles and dashed lines are estimated corrections.

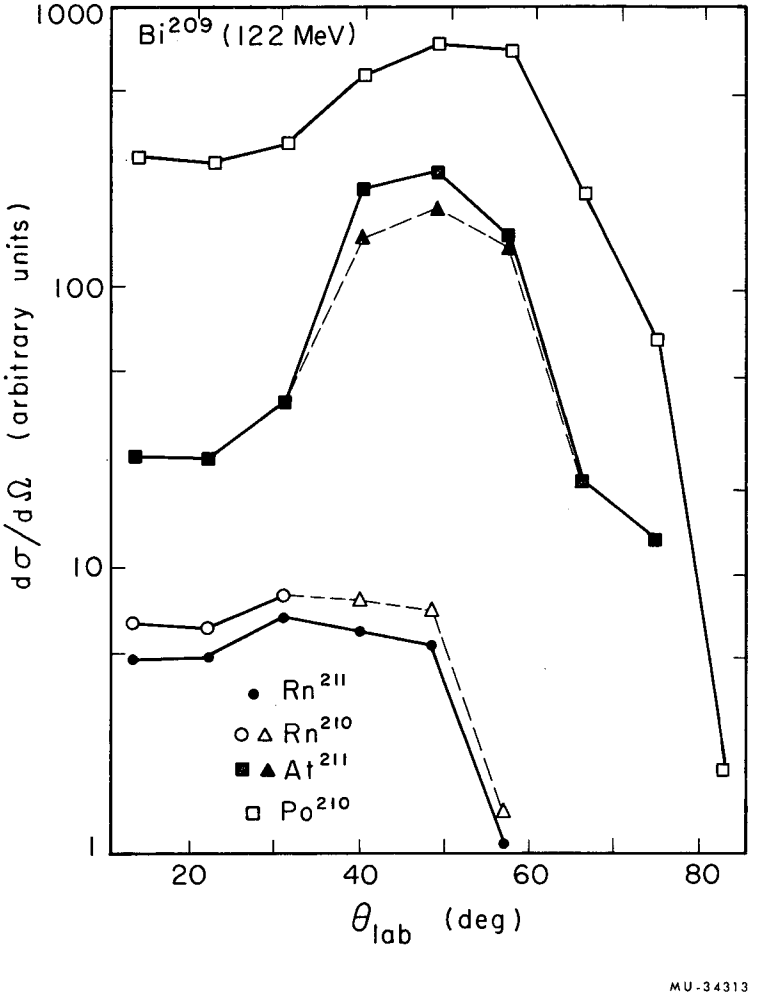

Fig. 14. Angular distributions. The differential cross section (arbitrary units) is plotted against the median angle of each collection segment. The circles, squares and solid lines are experimental data. The triangles and dashed lines are estimated corrections.

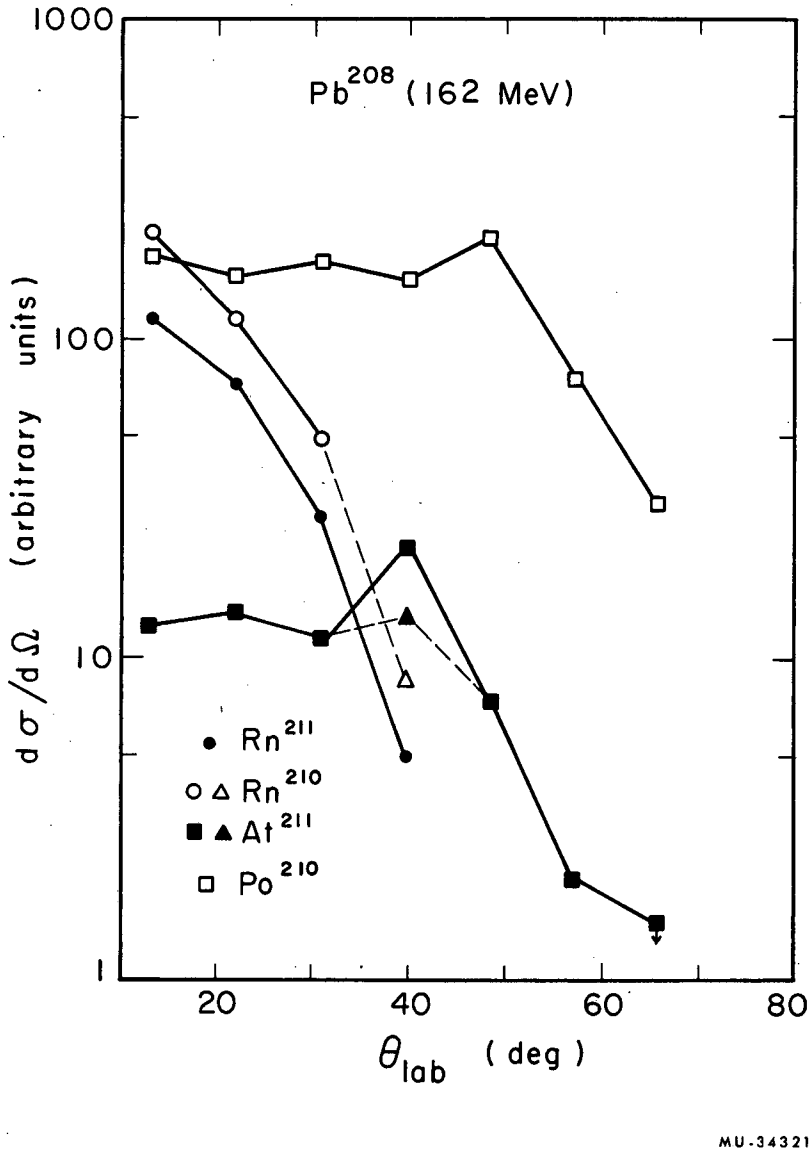

Fig. 15. Angular distributions. The differential cross section (arbitrary units) is plotted against the median angle of each collection segment. The circles, squares and solid lines are experimental data. The triangles and dashed lines are estimated corrections.

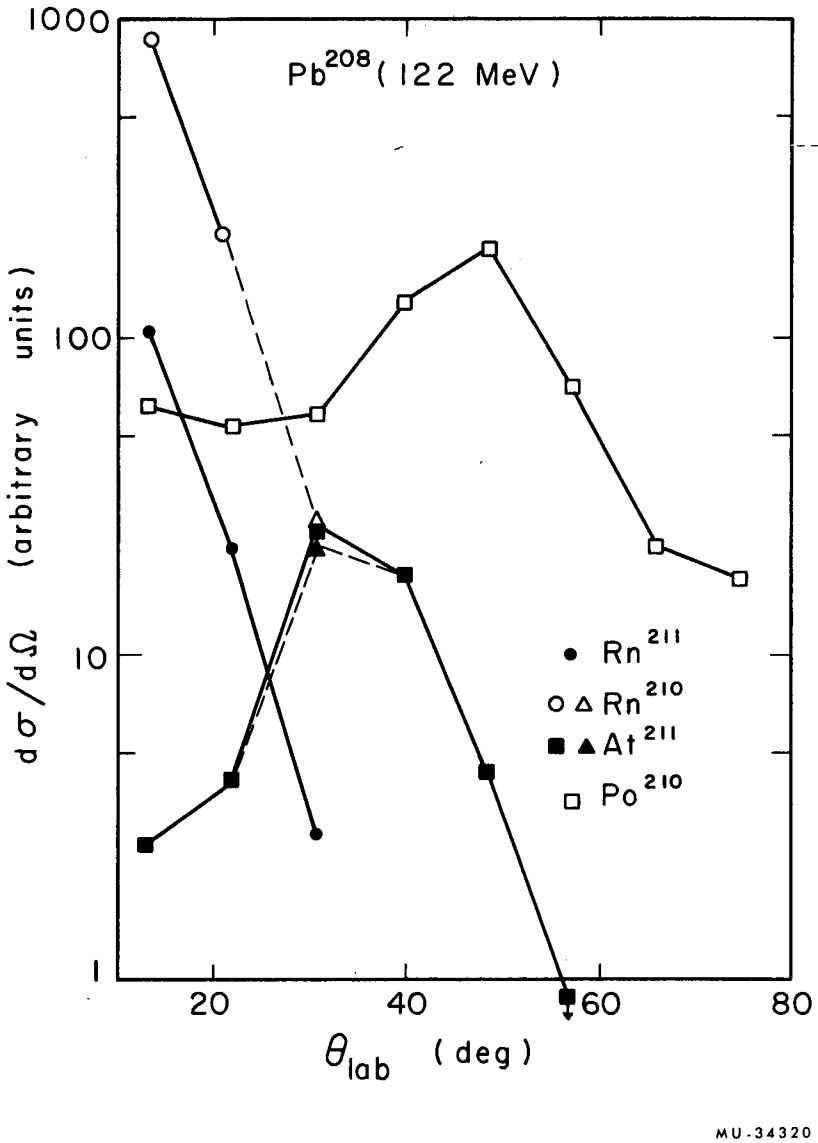

Fig. 16. Angular distributions. The differential cross section (arbitrary units) is plotted against the median angle of each collection segment. The circles, squares and solid lines are experimental data. The triangles and dashed lines are estimated corrections.

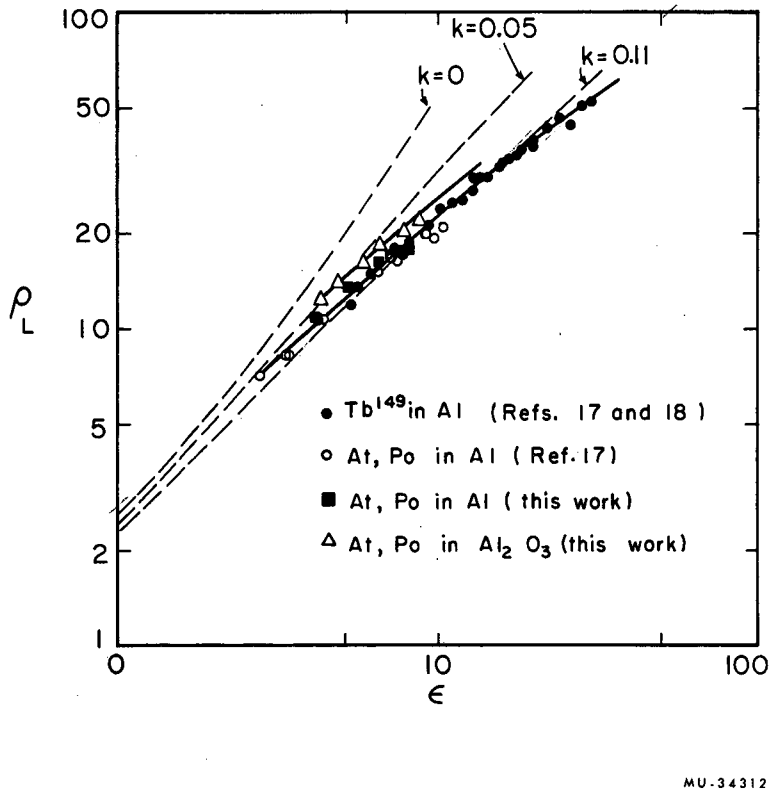

Fig. 17. Range-energy data from Fig. 4, re-plotted using the dimensionless variables ρ_L and ϵ. The dashed lines are theoretical predictions. See text.

Z \ N	122	124	126	128	130	132	134
							Pa^{225} *
90						Th^{223} *	Th^{224} *
						Ac^{221} *	Ac^{222} *	Ac^{223} 2.2 m α ε
88			Ra^{213} 2.7 m α			Ra^{214} *	Ra^{220} *	Ra^{221} *	Ra^{222} *
			Fr^{212} 19.3 m α(44%) ε			Fr^{217} *	Fr^{218} *	Fr^{219} *	Fr^{220} *	Fr^{221} 4.8 m α
86	Rn^{207} 11 m α(~30%) ε	Rn^{208} 23 m α(~20%) ε	Rn^{209} 30 m α(~17%) ε	Rn^{210} 2.42 h α(96%) ε	Rn^{211} 14.6 h α(28%) ε	Rn^{212} 25.5 m A(>99%)			Rn^{215} *	Rn^{216} *	Rn^{217} *	Rn^{218} *	Rn^{219} *	Rn^{220} *
	At^{206} 29 m α(~30%) ε	At^{207} 1.6 h α(~10%) ε	At^{208} 1.6 h α(0.5%) ε	At^{209} 5.5 h α(~5%) ε	At^{210} 8.3 h α(0.17%) ε	At^{211} 7.21 h α(41%) ε	At^{212} *	At^{213} *	At^{214} *	At^{215} *	At^{216} *	At^{217} *	At^{218} *	At^{219} *
84	Po^{205} 1.8 h α(~1%) ε	Po^{206} 8.8 d α(5%) ε	Po^{207} 6.2 h α(0.01%) ε	Po^{208} 2.9 y α(>99%)	Po^{209} 103 y α(~90%)	Po^{210} 138.4 d α(~100%)	Po^{211} 0.5 s α(~100%)	Po^{212} *	Po^{213} *	Po^{214} *	Po^{215} *	Po^{216} *	Po^{217} *	Po^{218} 3.05 m α
	Bi^{204} †	Bi^{205} †	Bi^{206} †	Bi^{207} †	Bi^{208} †	$\underline{Bi^{209}}$	Bi^{210} 5.0 d β^-(~100%)	Bi^{211} 2.2 m α(~100%)	Bi^{212} 60.5 α(~35%)	Bi^{213} 47 m α(2%)	Bi^{214} †	Bi^{215} †		
82	Pb^{203} †	$\underline{Pb^{204}}$	Pb^{205} †	$\underline{Pb^{206}}$	$\underline{Pb^{207}}$	$\underline{Pb^{208}}$	Pb^{209} †	Pb^{210} 21 y β^-	Pb^{211} †	Pb^{212} †		Pb^{214} †		

MUB-3615

Fig. 18. A portion of the Chart of the Nuclides. Stable isotopes are underlined. An asterisk denotes an α emitter with half life less than 1 min. A dagger indicates that no α-branching ratio greater than 0.1% has been reported. Half lives, decay modes and branching ratios are given for some nuclides. To conform to standard notation and to simplify the figure, the abbreviations used differ from those used elsewhere in this paper (e.g. h = hr = hour) and the symbol ε denotes electron capture. Data are from Refs. 9, 29, 41 and this work.

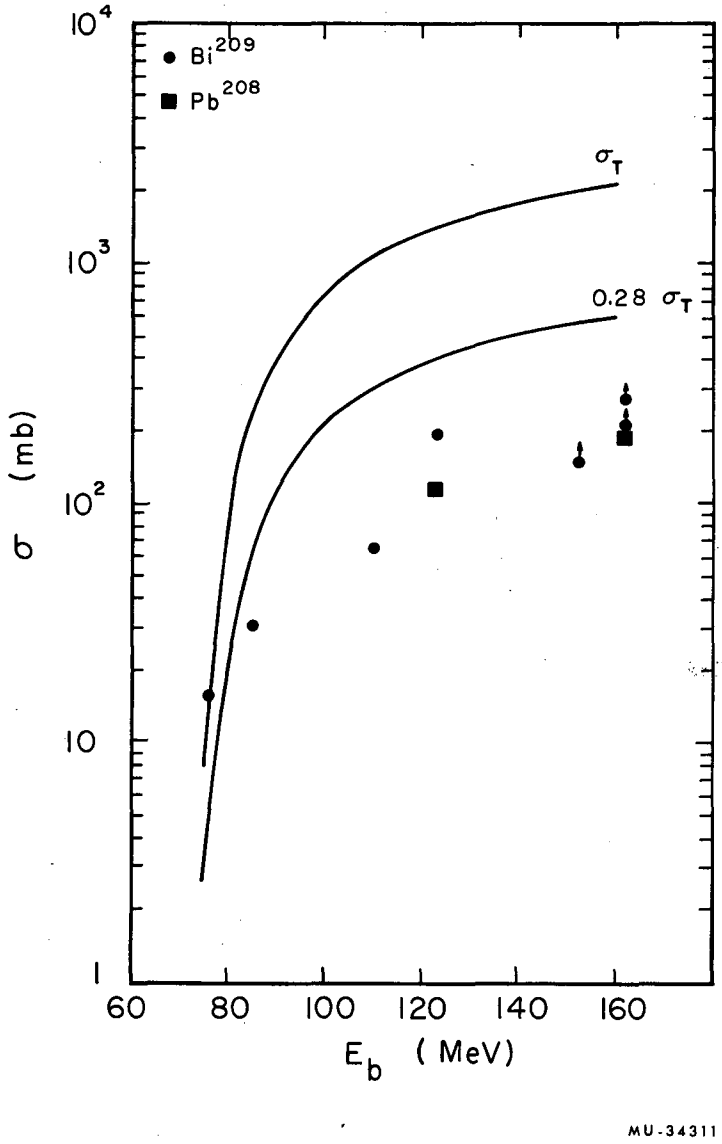

Fig. 19. Cross sections for bombardment of Bi^{209} and Pb^{208} with O^{16}. The upper curve is the total reaction cross section, σ_T, as interpolated from Thomas' tables.[11] The 0.28 σ_T curve is an estimate of the non-fission cross section (see text). The points represent the sum of the measured cross sections for all α emitters detected in this work.

APPENDICES

A. Analysis of Pulse-Height Spectra of Al_2O_3 Foils from Bi and Pb Bombardments

The analysis of the α spectra consisted of fairly straightforward and familiar techniques. The general method will be described first; there will follow a brief indication of the peculiarities of each product measured.

As was stated earlier, the α peaks in the spectra obtained were usually quite well separated from one another. Of the counts associated with a particular α-group, about 93% were situated within a well-defined peak with half width of 60-80 keV. (As described in Section II, the counter was capable of a resolution of less than 40 keV. The larger values obtained in practice presumably were caused by slight degradation of the α particles in the Al_2O_3 foils). A further 6% of the counts were found in a low energy exponential tail extending about 0.5 MeV below the peak. Inclusion of the next 0.8 MeV picked up about 1% more counts. Lower energy counts were neglected.

The composition figures for the peak and tail in the preceding paragraph were obtained from exhaustive analyses of the 7.44 MeV peak of Po^{211} which was situated well off by itself in the spectra. (Corrections were made for contributions from the 6.88 and 6.56 MeV branches). Most of the other peaks were not that isolated; usually at least one other peak would be found on the tail of the particular radiation under consideration, preventing simple summation of the 1.3 MeV region containing the pertinent counts. Therefore the usual procedure was to sum the counts in the peak alone and correct this value using the 0.93 factor obtained from the 7.44 MeV component. Contributions to a peak from the tail of a higher peak were frequently small, and were estimated by simple extrapolation in the obvious way.

The spectra were plotted on semi-log paper i.e. effectively (log of the number of counts) vs. (channel number). This made feasible the manufacture and use of a number of templates for 'peak shape' and 'tail shape', and these were used to guide the various extrapolations necessary. Although the above description may appear to imply frequent subjective judgments ("how wide is that peak?", "how high is that tail?"), the corrections involved were usually quite small, and even a large error in the placing of a template would produce a negligible change in the counting rate determined. This was true because the template was used only to provide peak shape at the low edges of the peak. Counts from the main peak were summed directly from the analyser print-out. An indication of the consistency of the treatment is seen in the fact that the decay curves of most components did not exhibit "point scatter" except that attributable to statistical errors of counting. Moreover, it should be pointed out that a consistent error, although affecting the cross section determined for a given product, should not disturb the activity distribution appreciably, as all foils would be subject to the same error.

For all products, except the mass-211 growth and decay system which is discussed below, the counting rates were plotted vs the time after bombardment on semi-log paper. Generally, very good straight lines resulted, so that the initial activity could be accurately obtained by extrapolation in the usual way. This initial activity, uncorrected for branching ratio, decay during bombardment, counting efficiency, etc., was used directly as a measure of the projected range distributions. Total cross sections could be estimated, using the total activity for a species summed over all foils, along with the other usual bombardment information.

The next sections contain more specific details concerning each product identified. Unless otherwise indicated, decay information came from Refs. 9, 29 and 41 (see also Table II).

Fr^{212}:

Only tentative identification could be made of Fr^{212}. In some runs a small peak at 6.4 MeV was seen; usually the activities were so low that there was time for only one or, at most, two determinations of the count rate. Thus half-life information is scant, the best estimate for the half life, $t_{1/2}$, in minutes being expressed as $10 < t_{1/2} < 25$. The reported data for Fr^{212} (19.3 min.; 6.34, 6.39, 6.41 MeV) correspond fairly closely to the experimental information.[43] The few data points available, then, were fitted with a 19.3 min. half life in order to obtain approximate initial activities. Statistical errors (defined as equal to $100/\sqrt{\text{No. of counts}}$ %) were of the order of 10% at the lowest, so the Fr^{212} data should be viewed with some reserve.

Rn^{212}:

All of the high energy runs produced a well-defined α peak at 6.26 MeV. Although the half life was short, there was usually sufficient activity to take two or three counts of the radiation from each foil. From 40 foils with three or more counts each, the value $t_{1/2} = 25.5 \pm 1.0$ min was derived, where the error is the standard deviation as estimated by the method given in Evans.[42] Previous workers gave the energy and half life of Rn^{212} as 6.26 MeV and 23 min.[43] The above activity was therefore assigned to Rn^{212}. There seemed to be no reason to prefer the previously reported half life so 25.5 min. was used. (See also Appendix B).

If the activity at 6.4 MeV discussed above was indeed Fr^{212}, then it would have contributed to the Rn^{212} peak through its 56% electron capture branching ratio. Correction for this was not made, due to the element of doubt surrounding the Fr^{212} assignment, but it would be less than 10% of the Rn^{212} activity in any given foil, if proven necessary. (Moreover, since the Fr^{212} distribution usually peaked rather close to the Rn^{212} peak, the disturbance of the Rn^{212} distribution would not be large.)

Rn^{210}:

In most of the runs a definite peak at 6.04 MeV was observed. Early in the counting period there was some (small) interference from the tail of the Rn^{212} and other short-lived activities, but after about two hours the 6.04 MeV peak was well isolated. From 35 determinations of the half life, the value 2.42 ± 0.05 hrs was obtained. Values previously reported for Rn^{210} were $t_{1/2}$ = 2.7 ± 0.2 hrs, $E_\alpha = 6.03_7$ MeV, branching ratio ~96% α.[44] Assignment of the experimental 6.04 MeV α group to Rn^{210} seemed clear. For cross section estimations, the 2.42 hr half life and the 96% branching ratio were used.

At^{209}:

A peak at 5.65 MeV was frequently observed. The contribution from the tails of higher peaks, specifically the three peaks of about 5.86 MeV from the 211 chain, was not at all trivial. A correction factor was estimated by making a template of the shape of the 5.86 MeV peak and tail after the 5.65 MeV activity had decayed away. This was assumed to be the shape of the 5.86 MeV peak early in the counting period, and corrections to the 5.65 MeV summation were made accordingly. These corrections ranged from 10% to 50% of the peak total. Hence, the decay curve for this activity showed substantially more scatter than others obtained in this work. The half lives were about 5 to 6 hrs. On this evidence, the activity was assigned to At^{209} and the points were fitted to the 5.5 hr activity previously reported to obtain the initial activities required.

Po^{210}:

The peak at 5.30 MeV decayed with a half life of 135-140 days. These figures correlate well with the previously reported values for Po^{210} (5.29_8 MeV; 138.40 days). Any Rn^{210}, At^{210}, Bi^{210} produced in the bombardment would also contribute to the Po^{210} through β^- decay or electron capture. The small (ca. 1%) correction due to Rn^{210} was made as the distribution of this product was known from its own peak. At^{210}

and Bi^{210} do not have appreciable α-branching ratios so that their contribution was unknown. The data labelled "Po^{210}" must then accurately be attributed to (At^{210} + Po^{210} + Bi^{210}).

Po^{208}:

Superimposed on the tail of the 5.30 MeV Po^{210} peak there was frequently observed another peak at 5.1 MeV. As the intensity of this second peak was less than 10% that of the Po^{210} peak, determination of the tail correction was difficult. The decay curve showed a good deal of scatter but the half life could be bracketed at 2 to 4 years. Assignment of this activity was made to Po^{208} (reported values: 5.10_8 MeV; 2.93 years; 99^+% α-branching ratio). Corrections to the Po^{208} total from decay of Rn^{212} were made. Contributions from electron capture from At^{208} were unknown; thus the "Po^{208}" data is, more correctly, (At^{208} + Po^{208}).

Po^{206}:

In the lead bombardments, a shoulder on the Po^{210} peak was observed. Through application of the appropriate template a peak of about 9 days half life and 5.2 MeV was separated. This was assigned to Po^{206} (previously reported: 5.21_8 MeV; 8.8 days; 8% α-branching). Corrections for contribution from α-decay of Rn^{210} were made, but contributions from Rn^{206} and At^{206} are unknown.

Rn^{211} and At^{211}:

Peaks at 7.44 MeV and about 5.86 MeV were observed in every bombardment. In the low energy runs, both peaks decayed with a half life of ~ 7.3 hrs ; for higher energies a component of about 15 hrs was also present. Association of these peaks with the Rn^{211}-At^{211}-Po^{211} decay chain was obvious. Since the half lives of Rn^{211} and At^{211} are so close together, this growth-and-decay system was not amenable to graphical analysis as were the other activities in this work. Therefore a computer program was used to resolve these two components.

The program, FRENIC, has been described many times before (see for example, Refs. 45 and 46). Briefly, it is an iterative least-squares procedure which fits each counting rate, y_i with the expression $\sum_{j=1}^{k} A_j \exp(-\lambda_j t_i)$ where A_j is the activity parameter, λ_j the decay constant, t_i the time at which the counting rate was measured and k the number of components—in this case, two. The program then provides final values A_j^o and λ_j^o by minimizing

$$\sum_{i=1}^{n} W_i \left[y_i - \sum_{j=1}^{k} A_j \exp(-\lambda_j t_i)\right]^2$$

where n is the number of data points and W_i a weighting factor. The A_j^o's obtained correspond to the intercepts in a graphical analysis, the λ_j^o's to the decay constants. The program allows any of the parameters A_j, λ_j to be held constant if desired. As part of the output, the program also prints the standard deviations of the final values of the parameters.

From 22 determinations of the At^{211} half life in the low energy bombardments, the value 7.25 ± 0.10 hrs was obtained, in good agreement with Appelman's value of 7.214 ± .007 hrs.[47] Appelman's value was accepted as correct and held constant in the computer analyses of the more complicated decay curves. As a first step, both intercepts and λ_{Rn} were allowed to vary as the program treated 49 decay curves of the 7.44 MeV group from the high energy bombardments. The values of λ_{Rn}^o were collected and averaged in two ways:

(a) $$m_a = \frac{1}{49} \sum_{i=1}^{49} \lambda_i$$

$$\text{(b)} \qquad m_b = \frac{\sum_{i=1}^{49} (s_i)^{-2} \lambda_i}{\sum_{i=1}^{49} (s_i)^{-2}}$$

where m is the mean, and s_i the standard deviation for λ_{Rn} provided by the computer. (Of the 49 determinations, 38 had $s_i < 0.10\ \lambda_{Rn}$; 43 had $s_i < 0.15\ \lambda_{Rn}$.) The two means differed by less than 0.2%, so λ_{Rn} was taken as $\frac{1}{2}(m_a + m_b)$ giving a half life for Rn^{211} of 14.6 ± 0.6 hrs, where the error was again estimated using the method in Evans.[42]

Momyer and Hyde gave the half life of Rn^{211} as 16 ± 1 hrs.[44] It was not clear what their error assignment meant, but it seems reasonable to state that the value obtained in this work is in substantial agreement with their figure. They also quote 1.0 ± 0.1 as the ratio of the 5.86 peak to the 7.44 peak; the value from this work was 1.03. Calculation of the α-branching of Rn^{211} is rather sensitive to this ratio, but as it happens, use of the Rn^{211} $t_{1/2}$ = 14.6 hrs, the ratio 1.03, and the At^{211} $t_{1/2} = 7.21_4$ hrs yields almost the same α-branching (28%) as that found by Momyer and Hyde using the Rn^{211} $t_{1/2}$ = 16 hrs, a ratio of 1.0, and an At^{211} $t_{1/2}$ = 7.3 hrs (26%).

There seemed to be no reason to prefer the previous values (see Appendix B) so the quantities determined in this work for Rn^{211} (14.6 hrs; 28% branching) were used in the decay-curve analysis. The data points were fed through the computer again, this time with both λ_{At} and λ_{Rn} fixed, to obtain the final intercept values. Standard deviations of the intercepts were usually around 3% or less.

Other Products:

Although certain other nuclides in this region of the periodic table have α activities which might have been seen in this work had they been present in sufficient quantity, no α groups other than the ones already discussed could be distinguished in the spectra. Various

other potential products are listed in Table X. Some have very low α-branching ratios; some have α energies such that their peaks, if low, would be swamped by the large count rate of another product. An estimate of the maximum possible count rate for each of these nuclides was made and the maximum possible cross section was calculated. Certain of these cross section estimates could be reduced through consideration of their contribution to other, measurable products by electron capture. (For example, a cross section of about 120 mb would be necessary before At^{208} could be detected through its own α radiation; however, since it decays to Po^{208}, obviously its cross section cannot exceed the value calculated from measurement of the Po^{208} radiation.) These estimated maximum possible cross sections are recorded in Table X.

B. Radon Diffusion

The fact that the half lives determined in this work for Rn^{210} and Rn^{211} were both about 10% below the corresponding values previously reported, might prompt some suspicions that Rn isotopes could be lost from the foil due to a diffusion or other leakage phenomonon. This possibility was considered but relegated to low importance for the following reasons.

(a) The half life for Rn^{213} in this work was about 10% greater than the previous value.

(b) The decay curves for Rn^{210} were rather good straight lines on semi-log paper. This suggests that the rate equation for any diffusion loss present is of the same form as for the loss by radioactive decay. If this is true, we can postulate a diffusion decay constant for radon, λ_d, in addition to the experimental and radioactive decay constants λ_e and λ_r respectively, where for λ_r we will use the previous value. Now $\lambda_e = \lambda_r + \lambda_d$.

For Rn^{210}: $\frac{0.693}{2.42} = \frac{0.693}{2.7} + \lambda_d$ or $\lambda_d = 0.03\ hr^{-1}$

For Rn^{211}: $\frac{0.693}{14.6} = \frac{0.693}{16} + \lambda_d$ or $\lambda_d = 0.004\ hr^{-1}$

That is, the diffusion decay rates are vastly different for Rn^{210} and Rn^{211}; this would appear to be an unreasonable possibility.

(c) For one of the bombardments, the most active foil was stored under vacuum (~ 10^{-4} mm Hg) at 122°C at all times that it was not actually in the counter. The half life for Rn^{210} in this foil was about one minute less than the 2.42 hr average value, a difference of under 1%. It is difficult to imagine a diffusion process which would be so independent of temperature changes.

(d) Even if a diffusion-type loss does occur from the foils, the fact that the decay curves were extrapolated back to the initial activities using the actual experimental half lives ensures that the initial activities were correct. And it was these initial activities which were used to define the range distribution curves.

For all of the above reasons, then, loss of radon from the foils due to diffusion was judged to have a negligible effect on the results.

(It must be admitted that the above arguments do not apply to loss from the foils while they are situated in the beam. Deposition of energy in such thin foils is, of course, very small. On the other hand, Al_2O_3 is not a good thermal conductor. Although the holder and stainless steel rings were maintained at ~15°C. during the bombardment by the cooling water flow, the 3/16 in. diameter circle through which the beam passed and in which many of the recoils lodged could have reached a high temperature. This might have allowed some diffusion, particularly of radon.)

C. Errors

Estimates of the errors involved in some of the measurements taken during this work are given in the following paragraphs. No attempt has been made to provide an accurate set of error limits for each of the hundreds of quantities measured; it is hoped, however, that sufficient information is furnished that the concerned reader will be able to make his own judgement as to the degree of confidence deserved by a given measurement.

Projectile beam. Alexander and Simonoff found that day to day variations in the beam energy were probably less than ± 3/4%.[48] The beam energy width has been given by Hubbard et al. as 2% (full width half maximum).[23] Beams used in this work were always bent 30° after exit from the machine; this should have the effect of lowering the beam spread somewhat, but this was not measured quantitatively. An estimate of the beam spread after degradation can be obtained from McIntyre and co-workers who show that the energy spread increases by the ratio of the dE/dR after degradation to the dE/dR before.[49,50] Use of this relationship and the dE/dR values as measured by Northcliffe, yields a beam spread of less than 7% for 80 MeV O^{16}.[24]

Targets. O'Connell and co-workers, who made most of the targets used in this work claim knowledge of the thickness to within 5%.[51] Counting of the Po^{210} activity naturally occurring in the Pb^{208} targets indicated that, if anything, this figure is too pessimistic. Since target corrections for the range distribution measurements were so small, errors in the target thickness itself are negligible.

O^{16} on Ir; Al leaf catchers. The Al leaf foils were each weighed at least twice before use and the results averaged. The standard deviation of the weighings was ± 1%. In addition to this error, there was an average gradation in thickness of 9 $\mu g/cm^2$ per cm; thus, for a one inch foil, the thickness would vary, on the average, about 15% across the entire foil. The thickness obtained by dividing the

weight by the area would then be about 7.5% different from the thickness at the edge. Since the recoils passed through a number of foils, these errors would tend to be self-cancelling to some extent. Errors in determining the activities of the foils should not be more than 3% for the peak foils, and perhaps 5 to 8% out in the tails of the distribution. The error in reading the probability plots is perhaps 1 to 2% for R_m and thus about 10% for ρ. Finally, let us allow 1% for possible error in the small target correction applied.

<u>O^{16} on Ir; Al_2O_3 catchers</u>. The four thickness-per-volt factors from the literature for Al_2O_3 production covered a range of only 1.1%.[25-28] The voltage was controlled to 148 ± 1 volt. If we add another 1% error for the effect of other variables, we see that the foils should be alike to within about 2% and their thickness should be known to within about 3%. Activity determination errors were the same as for the Al leaf experiments just described; since the probability plots were better straight lines for Al_2O_3, the reading error is probably lower than for Al leaf; the target correction error is about the same.

<u>O^{16} on Bi, Pb^{208}; Al_2O_3 catchers</u>. Errors in the distribution curves stem chiefly from the small foil thickness errors described above and also the counting statistics which, of course, vary widely from product to product and foil to foil. Errors on the high counting peaks were under 3%; errors on the lower activities and/or those complicated with large tail corrections (e.g., At^{209}, $Po^{206,208}$; see Appendix A) could reach 50%. A good estimate of the scatter can be obtained simply by examining for smoothness the distributions listed in Table III or shown in Figs. 7 to 10. The R_p values could be obtained to within 10%. R_m values could be read off the curved probability plots to within 5% and R_a values would have errors of similar magnitude. However, as was described earlier, R_m, and especially R_a, are sensitive to the depth in the foil stack to which the long range tail could be followed, and could be up to 5 to 10% low for some products of low activity.

An idea of the reproducibility of the range distributions and ranges can be gained from a comparison of Runs I and II, which had the same bombarding energy. It must be kept in mind that Run I was carried out earliest of all the experiments reported here, the target was rather thick, and the measurements were taken with equipment generally inferior to that available later. These considerations may explain some of the discrepancies.

Angular Distribution Experiments. The fact that these experiments were subject to large error has been mentioned and discussed briefly in Section II-D. The long Al leaf strips used as catchers were not weighed individually; their thickness was taken as the average thickness of a large number of circular foils punched from the same package of leaf. The standard deviation in the thickness was estimated using the method of Evans to be ± 9%.[42] Cutting of the foil stack into angular segments was accurate to within 5%. Counting statistics, due to the low activities and short half lives were rarely better than 5% and were frequently worse than 10%. Analysis of the decay curves were probably good to only about ± 15%, although some of this would be a consistent error, which would not affect the shapes of the angular and range distributions as much as their magnitude. Thus, the error in a single point might be as high as 30 to 35%. The "averaging" method used to extract $\overline{R}_{proj}$ apparently reduced the error in this quantity to around 10%, as was described earlier. (Section II-D). Presumably the error in R_{θ_p} would be approximately the same.

Cross Sections. A bombardment designed to measure the cross section for a short-lived product is frequently quite different from one designed to measure long-lived products. The large amount of work involved in the preparation, counting, and, especially, data processing associated with one of the bombardments in this work made the prospect of separate runs for short- and long-lived products extremely unattractive. Therefore the cross sections quoted are only approximate values.

(A rationalization of this attitude is that since a number of mechanisms are apparently contributing to the formation of each product, the possession of an accurate gross excitation function is not particularly valuable.) Most of the values given should be good to ~± 30%. As mentioned earlier, there was some target loss in the high energy runs, so that those cross sections are almost certainly low, perhaps by 50%. Within a given run, relative cross sections should be somewhat more accurate except that the short-lived Fr^{212} and Rn^{212} may be in larger error due to the difficulty with the decay-during-bombardment correction.

75.8 MeV Bi Bombardment. Table XI shows the possible effects of various errors on the energy-momentum calculations for the low energy Bi bombardment. The first three lines show the E*'s as calculated in Section III with E_b = 75.8 MeV and zero impact parameter. As was described there, the α transfer reaction is energetically impossible, the 2p transfer reaction may leave slightly too much excitation energy to produce an At^{211}, and the single p transfer yields Po^{210} directly. The beam spread at 75.8 MeV is about 5.4 MeV (FWHM) as described earlier in this Appendix. Lines 4 to 6 in the table show the E*'s resulting from interactions of the projectiles of energy 78.5 MeV. Alpha transfer is now possible, but cannot lead to At^{211} as an $E^* \gtrsim 10.9$ is required to remove the two neutrons. Both p and 2p transfer reactions now deposit too much excitation energy for Po^{210} and At^{211} to remain as final products. This might be disconcerting (as there is certainly an appreciable number of beam particles with energies 78.5 and above) were it not for the information provided in lines 7 and 8 of the table.

Here, the impact parameter is no longer assumed to be zero, but the recoils are allowed to come off at small angles. Equations (10) are now used to calculate the E* values and, of course, for E_R we must now use the energy obtained from (projected range times sec θ). Clearly, at even small impact parameters, energy transfer is sufficiently reduced that the E* values drop into the acceptable range. Thus, the beam

spread presents no problem; the high energy fraction of the beam simply reacts at slightly larger impact parameters to produce At^{211} and Po^{210}.

Line 9 to Table XI shows that E_b must be 83.7 MeV before α transfer can produce At^{211} even at zero impact parameter. There should be few particles of this energy in the beam.

Of course, an error in the determination of E_R would also affect the calculation. It will be recalled that the extrapolation of the range-energy curve for Al_2O_3 was drawn parallel to the Al curve. A close examination of the points plotted in Figs. 4 and 17 suggests that, if this extrapolation is in error, it probably lies too high on the graph. That is, for a given range, the recoil energy derived from the extrapolated curve may be too low. Lines 9 and 10 of Table XI show the effect of increasing the measured E_R's by 5%. The result for Po^{210}—a negative E*—may be taken to indicate that the E_R is <u>not</u> in error to this extent. The single p transfer process with the N^{15} emitted directly backwards is the most efficient momentum transfer possible. Line 12 shows that 18.5 MeV is the largest $E_{Po}210$ kinematically possible. (Perhaps it should be mentioned that the presence of Po^{210} in the long range tail of the range distribution beyond E_R = 18.5 does not imply kinematic impossibility. The spread in the range distribution can be attributed to stopping straggling; the ρ values (~ 0.17) appear quite reasonable).

To sum up, the above considerations all show that α transfer cannot account for the production of At^{211} and Po^{210} near the barrier, but that assumption of p and 2p transfer mechanisms leads to a consistent picture.

FOOTNOTES AND REFERENCES

1. A Zucker, Ann. Rev. Nucl. Sci. 10, 27 (1960).
2. K. S. Toth and E. Newman, Phys. Rev. 130, 536 (1963). The bibliography of this paper contains a number of references to single-nucleon transfer studies.
3. G. Breit and M. E. Ebel, Phys. Rev. 103, 679 (1956).
4. G. Breit and M. E. Ebel, Phys. Rev. 104, 1030 (1956).
5. Richard Kaufmann and Richard Wolfgang, Phys. Rev. 121, 192 (1961).
6. M. L. Halbert, T. H. Handley, J. J. Pinajian, W. H. Webb and A. Zucker, Phys. Rev. 106, 251 (1957).
7. H. C. Britt and A. R. Quinton, Phys. Rev. 124, 877 (1961).
8. S. N. Shumilov, A. P. Klyucharev and N. Ya. Rutkevich, Zh. Eksperim. i Teor. Fiz. 45, 1356 (1963). [Trans: Sov. Phys. JETP, 18, 934 (1964).]
9. D. T. Goldman, G. E. Chart of the Nuclides, 6th Edition, 1962.
10. V. E. Viola, Jr., and T. Sikkeland, Phys. Rev. 128, 767 (1962).
11. T. D. Thomas, Phys. Rev. 116, 703 (1959).
12. B. Wilkins and G. Igo, Proceedings of the Third Conference on Reactions Between Complex Nuclei, Asilomar (Berkeley: University of California Press, 1963) p. 241.
13. T. Sikkeland, E. L. Haines and V. E. Viola, Jr., Phys. Rev. 125, 1350 (1962).
14. T. Sikkeland and V. E. Viola, Jr., Proceedings of the Third Conference on Reactions Between Complex Nuclei, Asilomar (Berkeley: University of California Press, 1963) p. 232.
15. H. C. Britt and A. R Quinton, Phys. Rev. 120, 1768 (1960).
16. John M. Alexander and Lester Winsberg, Phys. Rev. 121, 529 (1961).
17. Lester Winsberg and John M. Alexander, Phys. Rev. 121, 518 (1961).
18. John M. Alexander and David H. Sisson, Phys. Rev. 128, 2288 (1962).
19. Morton Kaplan and Richard D. Fink, Phys. Rev. 134 B30 (1964).
20. Morton Kaplan, Phys. Rev. 134, B37 (1964).
21. J. B. J. Read, I. Ladenbauer-Bellis and R. Wolfgang, Phys. Rev. 127, 1722 (1962).

22. I am grateful to Dr. R. D. MacFarlane whose persistence in extolling the virtues of Al_2O_3 films overcame my initial skepticism.

23. E. L. Hubbard et al., Rev. Sci. Instr. 32, 621 (1961).

24. L. C. Northcliffe, Phys. Rev. 120, 1744 (1960).

25. Louis Harris, J. Opt. Soc. Am. 45, 27 (1955).

26. W. Walkenhorst, Naturwissenschaften 34, 373 (1947).

27. J. R. Young, Phys. Rev. 103, 292 (1956).

28. J. A. Davies, J. Friden, and J. D. McIntyre, Can. J. Chem. 38, 1526 (1960).

29. D. Strominger, J. M. Hollander, and G. T. Seaborg, Rev. Mod. Phys. 30, 585 (1958).

30. L. C. Northcliffe, Ann. Rev. Nucl. Sci. 12, 67 (1963).

1 photocopy → 31. J. Lindhard, M. Scharff and H. E. Schiøtt, Kgl. Danske Videnskab. Selskab, Mat.-Fys. Medd. 33, No. 14 (1963).

32. J. Gilat and J. M. Alexander, Stopping of Dysprosium in Gases and Aluminum, (UCRL-11055, January 1964) to be published in Phys. Rev.

33. P. G. Roll and F. E. Steigert, Nucl. Phys. 17, 54 (1960).

34. G. R. Piercy, F. Brown, J. A. Davies and M. McCargo, Phys. Rev. Letters 10, 399 (1963). In this work, the crystalline nature of the Al used allowed some lattice tunneling effects which extended the Al ranges; hence, the Al/Al_2O_3 comparison is not conclusive.

35. If R is expressed in mg/cm^2 the abundances should be calculated by weight (here $x_{Al} = 0.53$, $x_O = 0.47$).

36. J. M. Alexander, J. Gilat, and D. H. Sisson, Neutron and Photon Emission from Dysprosium and Terbium Compound Nuclei: Range Distributions, (UCRL-11187, March 64) to be published in Phys. Rev.

37. Richard Kaufmann and Richard Wolfgang, Phys. Rev. 121, 206 (1961).

38. Marshall Blann and Alan Ewart, Phys. Rev., 134, B783 (1964).

39. E. Lozhinski, Experimental Investigation of Angular Distribution in Transfer Reactions with Ne^{20} and Ar^{40} ions, Joint Institute for Nuclear Research (Dubna, USSR) Report JINR-P-1486. (Trans: UCRL-Trans-1080).

41. W. H. Sullivan, Trilinear Chart of Nuclides, (Oak Ridge National Laboratory, revised 1962).

42. Robley D. Evans, The Atomic Nucleus (McGraw-Hill Book Co., Inc., New York 1955) p. 903.

43. E. K. Hyde, A. Ghiorso, and G. T. Seaborg, Phys. Rev. 77, 765 (1950).

44. F. F. Momyer, Jr., and E. K. Hyde, J. Inorg. Nucl. Chem. 1, 274 (1955).

45. G. R. Keepin, R. F. Wimeth and R. K. Zeigler, J. Nucl. Energy 6, 1 (1957).

46. H. Marshall Blann, Fission of Gold with 112 MeV C^{12} Ions (Ph.D. Thesis) Lawrence Radiation Laboratory Report, UCRL-9190 (unpublished).

47. E. H. Appelman, Phys. Rev. 121, 253 (1961).

48. John M. Alexander and G. S. Simonoff, Phys. Rev. 130, 2313 (1963).

49. L. C. Becker, G. K. Tandon, F. C Jobes, J. A McIntyre and T. L. Watts, Nucl. Instr. Methods 21, 298 (1963).

50. J. A. McIntyre, T. L. Watts, and F. C. Jobes, Nucl. Instr. Methods 21, 281 (1963).

51. Daniel J. O'Connell, Lawrence Radiation Laboratory (private communication).

52. H. Kumpf and E. O. Donets, Zh. Eksperim. i Teor. Fiz. 44, 798 (1963). [Trans: Sov. Phys. JETP 17, 539 (1963).]

This report was prepared as an account of Government sponsored work. Neither the United States, nor the Commission, nor any person acting on behalf of the Commission:

A. Makes any warranty or representation, expressed or implied, with respect to the accuracy, completeness, or usefulness of the information contained in this report, or that the use of any information, apparatus, method, or process disclosed in this report may not infringe privately owned rights; or

B. Assumes any liabilities with respect to the use of, or for damages resulting from the use of any information, apparatus, method, or process disclosed in this report.

As used in the above, "person acting on behalf of the Commission" includes any employee or contractor of the Commission, or employee of such contractor, to the extent that such employee or contractor of the Commission, or employee of such contractor prepares, disseminates, or provides access to, any information pursuant to his employment or contract with the Commission, or his employment with such contractor.